THE PLANT CELL

Research Article

Spatiotemporal formation of the large vacuole regulated by the BIN2-VLG module is required for female gametophyte development in Arabidopsis

Li-Qin Hu [1,2,3,†] Shi-Xia Yu [1,2,3,†] Wan-Yue Xu [4] Song-Hao Zu [1] Yu-Tong Jiang [1] Hao-Tian Shi [2,3] Yan-Jie Zhang [1] Hong-Wei Xue [2,3] Ying-Xiang Wang [4] and Wen-Hui Lin [1,2,*]

1 School of Life Sciences and Biotechnology, The Joint International Research Laboratory of Metabolic and Developmental Sciences, Shanghai Jiao Tong University, Shanghai 200240, China
2 Shanghai Collaborative Innovation Center of Agri-Seeds/Joint Center for Single Cell Biology, Shanghai Jiao Tong University, Shanghai 200240, China
3 School of Agriculture and Biology, Joint Center for Single Cell Biology, Shanghai Jiao Tong University, Shanghai 200240, China
4 State Key Laboratory of Genetic Engineering and Ministry of Education Key Laboratory of Biodiversity Science and Ecological Engineering and Institute of Biodiversity Sciences, Institute of Plant Biology, Center for Evolutionary Biology, School of Life Sciences, Fudan University, Shanghai 200240, China

*Author for correspondence: whlin@sjtu.edu.cn (W.-H.L.)
†These authors contributed equally.

Abstract

In *Arabidopsis thaliana*, female gametophyte (FG) development is accompanied by the formation and expansion of the large vacuole in the FG; this is essential for FG expansion, nuclear polar localization, and cell fate determination. Arabidopsis VACUOLELESS GAMETOPHYTES (VLG) facilitates vesicular fusion to form large vacuole in the FG, but the regulation of *VLG* remains largely unknown. Here, we found that gain-of-function mutation of *BRASSINOSTEROID INSENSITIVE2* (*BIN2*) (*bin2-1*) increases VLG abundance to induce the vacuole formation at stage FG1, and leads to abortion of FG. Loss-of-function mutation of *BIN2* and its homologs (*bin2-3 bil1 bil2*) reduced VLG abundance and mimicked *vlg/VLG* phenotypes. Knocking down *VLG* in *bin2-1* decreased the ratio of aberrant vacuole formation at stage FG1, whereas FG1-specific overexpression of *VLG* mimicked the *bin2-1* phenotype. *VLG* partially rescued the *bin2-3 bil1 bil2* phenotype, demonstrating that *VLG* acts downstream of *BIN2*. Mutation of VLG residues that are phosphorylated by BIN2 altered VLG stability and a phosphorylation mimic of VLG causes similar defects as did *bin2-1*. Therefore, BIN2 may function by interacting with and phosphorylating VLG in the FG to enhance its stability and abundance, thus facilitating vacuole formation. Our findings provide mechanistic insight into how the BIN2-VLG module regulates the spatiotemporal formation of the large vacuole in FG development.

Open Access

IN A NUTSHELL

Background: In Arabidopsis, the development of the female gametophyte (FG) within the ovule is essential for plant reproduction and seed yield. Formation of the large vacuole within the FG is required for FG expansion, nuclear polar localization, and cell fate determination, which is critical for successful double fertilization. Generally, the large vacuole is visible after the first nuclear division during FG development. VACUOLELESS GAMETOPHYTES (VLG) regulates FG development by facilitating vesicular fusion to form large vacuole, but how VLG is regulated in this process remains unclear.

Question: How does the spatiotemporal formation of the large vacuole influence Arabidopsis FG development? How is VLG function regulated during FG development?

Findings: *BRASSINOSTEROID INSENSITIVE2* (*BIN2*) is expressed in the FG and localizes in vesicular-like structures. Increased BIN2 activity (in the gain-of-function mutant *bin2-1*) enhances VLG stability through preventing its degradation by the 26S proteasome; the increase in VLG promotes large vacuole formation at stage FG1. Decreased BIN2 activity (in the loss-of-function mutant of *BIN2* and its homologs *bin2-3 bil1 bil2*) reduces VLG stability, which decreases vacuole formation at stage FG2. Both conditions impair FG development. Overall, our study revealed that the spatiotemporal formation of large vacuoles regulated by the BIN2-VLG module is required for normal FG development.

Next Step: Further studies will elucidate mechanisms by which early formation of the large vacuole disturbs nuclear division and FG development. We speculate that it changes the condition of organelles and micro-environment of the functional megaspore at stage FG1. So, we will further study how the first nuclear division of FG is affected. This work could contribute to understanding how FG development is triggered after the functional megaspore formed.

Introduction

In *Arabidopsis thaliana*, the female gametophyte (FG) within the ovule is required for successful double fertilization, which critically affects seed number and yield. The diploid megaspore mother cell (MMC) undergoes meiosis and generates four haploid megaspores, three of which degenerate. The surviving functional megaspore (FM) undergoes three rounds of syncytial nuclear division, vacuole formation and expansion, followed by nuclear migration, cellularization, and differentiation, eventually giving rise to the mature FG, which includes one egg cell, one central cell, and two synergid cells (Webb and Gunning, 1990; Modrusan et al., 1994; Schneitz et al., 1995; Christensen et al., 1997). Therefore, the nuclear division of the FM (i.e. the first nuclear division of the developing FG at stage FG1) is critical for the initiation of FG development.

Recently, genetic studies have identified gametophytic mutations that have begun to elucidate the genetic and molecular details of the initiation of FG development. Mutations in genes that are involved in the first nuclear division in Arabidopsis, including a classical ARABINOGALACTAN PROTEIN 18 (AGP18) (Acosta-Garcia and Vielle-Calzada, 2004), a spindle checkpoint protein BUDDING UNINHIBITED by BENZIMIDAZOLE (BUB3.1) (Lermontova et al., 2008), the only KINESIN-1 member of Arabidopsis (AtKIN-1) (Wang H et al., 2014), a nucleoporin Nup88-homolog MODIFIER of SNC1,7 (MOS7) (Park et al., 2014), HISTONE ACETYLTRANSFERASE 1 (HAT1) and HAT2 (Latrasse et al., 2008), CHROMATIN-REMODELING 11 (CHR11) (Huanca-Mamani et al., 2005), and MADS-box transcription factor AGAMOUS-LIKE 23 (AGL23) (Colombo et al., 2008), all result in FG development arrested at the one-nucleate stage. In addition, GA-dependent degradation of RGA-LIKE1 (RGL1) is essential for mitotic divisions of FM (Gomez et al., 2020). In somatic ovule tissues, small RNA silencing pathways mediated by ARGONAUTE5 (AGO5) positively control the first nuclear division (Tucker et al., 2012). KARYOPHERIN ENABLING the TRANSPORT of the CYTOPLASMIC HYL1 (KETCH1) interacts with the ribosomal protein RPL27a and promotes its accumulation in the nucleus, involving in ribosome biogenesis and translational capacity during the first nuclear division (Xiong et al., 2020). Targeted degradation of the INHIBITOR of CYCLIN-DEPDENT KINASE4/KIP-RELATED PROTEIN6 (ICK4/KRP6), which accumulates during meiosis, by Ring-type E3 ligases is essential for the interphase progression during mitotic cell cycle in FM (Liu et al., 2008). Also, the canonical SOLUBLE NSF ATTACHMENT PROTEIN (α-SNAP) in Arabidopsis, which is involved in the disassembly of SNARE complexes to mediate fusion of vesicles with target membranes, is also critical for the first nuclear division (Liu et al., 2021). However, the underlying molecular mechanisms and genetic control of how the first nuclear division is triggered are still largely unknown.

FG development is accompanied by vacuole formation and expansion, which are essential for FG expansion, nuclear polar localization, and cell fate determination. Generally, extremely small vacuoles (<1 μm) are present at late stage FG1 (Schneitz et al., 1995; Christensen et al., 1997). Shortly after the first nuclear division, several small vacuoles

(<5 μm) appear at various positions at early stage FG2, and these gradually coalesce in the center of the cell, forming the central vacuole at late stage FG2. Subsequently, the central vacuole expands, positioning the two nuclei at the chalazal and micropylar poles, respectively, a critical step for the pattern formation of the 4n + 4n embryo sac at stage FG5 (Schneitz et al., 1995; Christensen et al., 1997). Moreover, the polar localization of the large vacuole formed in the egg, synergid, and central cells facilitates double fertilization and is involved in establishing apical-basal polarity during embryogenesis (West and Harada, 1993; Schneitz et al., 1995; Christensen et al., 1997).

Previous studies have indicated that *VLG* encodes a divergent C1 (DC1) domain (cysteine-rich and histidine-rich zinc finger)-containing protein localized in multivesicular bodies (MVBs) or pre-vacuolar compartments (PVCs), promoting vesicular fusion to form a large vacuole in the FG. The *vlg/VLG* mutant has pleiotropic defects in FG development, including arrest at stages FG1 or FG2, lack of a large central vacuole at stage FG5, or collapsed FG at stage FG7 (D'Ippólito et al., 2017). In addition, the auxin biosynthetic gene *YUCCA8* is essential for the formation of a large vacuole (Panoli et al., 2015), and auxin efflux controls orderly nucellar degeneration around the FG, promoting central vacuole expansion (Wang et al., 2021). Besides, the FG of *cki1* (*CYTOKININ INDEPENDENT1, CKI1*) mutant is arrested at stage FG5 because of the absence of large central vacuole (Pischke et al., 2002). These results suggest that the large vacuole formation is indispensable for FG development; however, how vacuole formation is regulated remains largely unclear.

In this study, we found that *bin2-1*, a gain-of-function mutant of *BIN2* (Li et al., 2001), had abnormal vacuole formation during FG development. Enhanced BIN2 activity triggered early formation of a large vacuole at stage FG1, while reduced BIN2 activity impaired formation of the large vacuole at later developmental stages, both conditions eventually leading to FG abortion. Further investigation indicated that BIN2 interacted with and phosphorylated VLG, which stabilized VLG, thereby facilitating the large vacuole formation in the FG. Our findings suggest that the BIN2-VLG module regulates the spatiotemporal formation of the large vacuole that is essential for FG development. Our study identifies a key regulatory mechanism of vacuole formation, supporting the requirement for proper function of the large vacuole in FG development.

Results

Increased BIN2 activity leads to abnormal formation of large vacuoles at stage FG1

To study the developmental processes and regulatory mechanisms during formation of the FG, we observed FG development in mutants with reduced seed number per silique by confocal laser scanning microscopy. In autofluorescence images, the extremely bright, moderate bright and black represent nucleoli, cytoplasm and nucleoplasm, and vacuoles,

respectively, as described previously (Schneitz et al., 1995; Christensen et al., 1997; Shi et al., 2005). We found that *bin2-1* FGs exhibited aberrant vacuole formation at stage FG1. Normal *bin2-1* FGs consisted of nucleoli, cytoplasm, and nucleoplasm without visible vacuoles, consistent with wild-type FGs (Figure 1, A and B). However, approximately 43.6% (n = 188) contained large vacuoles, indicating they were aberrantly formed (Figure 1, C and Q). In addition, about 9% displayed nuclear degeneration, a percentage obviously higher than that of the wild-type (3%, n = 135) (Figure 1, D and Q). A previous report indicated that a gain-of-function *bin2-1* mutation led to a more active BIN2 kinase (Li and Nam, 2002). These results suggested that increased BIN2 activity resulted in aberrant formation of large vacuole and impaired FG development at stage FG1.

To examine whether the phenotypes were indeed caused by the *bin2-1* mutation, we constructed transgenic plants expressing the mutated *BIN2* gene containing the *bin2-1* mutation (named *BIN2**) that we recreated by site-directed mutagenesis, driven by the *SEEDSTICK* (*STK*) promoter (Li et al., 2001; Pinyopich et al., 2003; Kooiker et al., 2005; Matias-Hernandez et al., 2010; Zu et al., 2019). Twelve transgenic lines exhibited vegetative growth defects similar to *bin2-1*, and we randomly selected *#31* and *#32* lines for phenotypic analysis of FG development (Supplemental Figure S1A). Our data revealed that approximately 34.5% (n = 84) and 32.6% (n = 129) of FGs at stage FG1 generated aberrant vacuoles in *#31* and *#32*, respectively (Figure 1, E, F, H, I, and Q), while about 22.6% and 46.5% underwent degeneration in *#31* and *#32*, respectively (Figure 1, G, J, and Q). These results revealed that this mutated *BIN2* gene could induce formation of defective FGs similar to *bin2-1*.

To confirm that the abnormal vacuole defect arose from increased activity of BIN2, which is a GLYCOGEN SYNTHASE KINASE3 (GSK3)–like protein kinase, we exogenously applied the GSK3 kinase inhibitors bikinin and LiCl, to *bin2-1*, *#31* and *#32* plants (Klein and Melton, 1996; Stambolic et al., 1996; De Rybel et al., 2009; Rozhon et al., 2014). The frequency of FGs containing vacuoles at stage FG1 after bikinin treatment (14.8%, n = 66) and LiCl treatment (17.3%, n = 129) were significantly lower than that of the mock control (41.5%, n = 124) in *bin2-1* (Figure 1R). Similar results were also obtained for *#31* and *#32* (Figure 1R). These data indicated that exogenous GSK3 kinase inhibitors could partially restore the phenotype of FG at stage FG1 (containing aberrant large vacuoles in the *bin2-1* mutant and transgenic plants), and further supported the hypothesis that the abnormal large vacuole formation was caused by increased BIN2 activity.

Loss of BIN2 function results in defective female gametophyte development

BIN2 functions redundantly with its two closest homologs, *BIN2-LIKE1* (*BIL1*) and *BIL2* (Jonak and Hirt, 2002; Vert and Chory, 2006). Therefore, to explore whether loss of BIN2

Figure 1 Increased BIN2 activity leads to early formation of large vacuoles at stage FG1. (A–J) Confocal laser scanning microscopy images of developing FGs at stage FG1 in wild-type (A), *bin2-1* (B–D), and *ProSTK:BIN2*-GFP* transgenic lines #31 (E–G) and #32 (H–J). Normal FGs are shown in panels (A), (B), (E), and (H). Abnormal FGs with apparent vacuoles are shown in panels (C), (F), and (I). Abnormal FGs with degenerated nuclei are shown in panels (D), (G), and (J). (K) Normal FG at stage FG4 in wild-type. (L) Abnormal FG with one nucleus containing obvious vacuoles at stage FG4 in *bin2-1*. (M) Mature FG at stage FG7 in wild-type. (N–P) Aborted FGs in *bin2-1* (N), #31 (O), and #32 lines (P) at stage FG7. (Q) Percentages of abnormal FGs at stage FG1 in wild-type, *bin2-1*, #31 and #32 lines (R) Percentages of FGs containing vacuoles at stage FG1 in *bin2-1*, #31 and #32 lines following 10 μM bikinin and 10 mM LiCl treatments. FGs from three independent pistils were analyzed. (S) Percentages of abnormal FGs at stage FG7. Numbers indicate how many FGs were observed for calculating the ratio in (Q and S). FGs are outlined with dotted lines (A–C, E–F, H–I, and K–M). N represents the nuclei (A–C, E–F, H–I, K–L). DM represents the degenerating megaspores (A–J). AFG represents aborted FGs (N–P). CCN, ECN and SCN indicate the nuclei of central, egg, and synergid cells, respectively (M). FG, female gametophyte. V, vacuole. DFG, degenerated female gametophyte. FG1V, vacuoles formed at stage FG1. Error bars represent means ± SD. Statistically significant differences are tested by one-way ANOVA (**$P < 0.01$, Supplemental Data Set S2). Bars = 10 μm.

activity affects vacuole formation or FG development, we analyzed the *bin2-3 bil1 bil2* triple T-DNA insertion mutant, because the *bin2-3* single mutant has no obvious phenotype

(Vert and Chory, 2006; Yan et al., 2009). The results revealed that *bin2-3 bil1 bil2* FGs at stage FG1 were normal without visible vacuoles, consistent with observations of the wild-

type (Figure 2, A and B). At stage FG7, approximately 97.7% of wild-type FGs produced mature embryo sacs, while 2.3% degenerated ($n = 348$, Figure 2, C, D, and I). By contrast, 85.6% of bin2-3 bil1 bil2 FGs developed normally (in agreement with the wild-type), but 3.1% were arrested at stage FG1, 1.3% were arrested at stage FG2 lacking large vacuole, and 10.5% degenerated ($n = 229$, Figure 2, E–I). These results suggest that loss-of-function of BIN2 affects vacuole formation and FG development, implying that normal BIN2 function is important for FG development.

BIN2 is expressed in the female gametophyte

Because gain-of-function and loss-of-function mutants (triple mutant of BIN2 and its two homologs) of BIN2 have abnormal FG development, we analyzed whether BIN2 is expressed in the FG. To this end, we generated a GUS fusion construct driven by the BIN2 promoter as described previously (Li and Nam, 2002). The GUS staining assay results revealed ProBIN2:GUS expression in the FG from stage FG1 to stage FG7 (Supplemental Figure S2A). To further document the localization of BIN2 in the FG, an immunolocalization assay was performed using an anti-BIN2 antibody. Immunoblot analysis was conducted to examine the specificity of the anti-BIN2 antibody, and the results revealed that BIN2 ($\approx$43 kDa) was detected by the anti-BIN2 antibody in total protein extracts from wild-type plants (Supplemental Figure S2B). This result is consistent with previous reports that BIN2 has both phosphorylated and dephosphorylated forms in vivo (Kim et al., 2009; Li et al., 2020). Furthermore, the immunolocalization assay revealed that BIN2 was found in wild-type root cells but was hard to observe in those of the bin2-3 bil1 bil2 triple mutant (Supplemental Figure S2C).

In addition, the BIN2-GFP localization pattern in the ProBIN2:BIN2-GFP transgenic plant detected by the anti-GFP antibody was similar to that in the wild-type detected by the anti-BIN2 antibody (Supplemental Figure S2C). The above experiments indicated the effectiveness of the anti-BIN2 antibody. Thus, our immunolocalization assays in the FG revealed that BIN2 was detected in wild-type plants but was almost undetectable in bin2-3 bil1 bil2 triple mutant (Supplemental Figure S2, D and E), suggesting BIN2 becomes localized in the FG. Given that mutation of BIN2 leads to vacuole defects in the FG and that BIN2 is present in a punctate pattern (Supplemental Figure S2, D and E), we speculated that BIN2 localization might be related to the MVBs or PVCs, which could be fused with the vacuole (Cui et al., 2016, 2020). Further investigation showed the partial overlap of signals of BIN2 and GFP-VAMP711, a vesicle and tonoplast-expressed marker (Ebine et al., 2011; Feng et al., 2017) (Figure 2, J and K, Supplemental Figure S3), indicating that BIN2 might partially co-localize with GFP-VAMP711. Taken together, we speculate that BIN2 partially localizes in MVBs/PVCs in FG and likely functions in vacuole-related FG development.

The large vacuoles are formed early in bin2-1 female gametophyte development

To investigate whether the vacuole defect seen in bin2-1 FG resulted from early developmental processes, we analyzed the expression of marker genes in the MMC (ProKNU:KNU-VENUS) (Payne et al., 2004; Zhao et al., 2018) and FM (ProFM1:GUS) (Huanca-Mamani et al., 2005). Expression of KNU and FM1 was not altered in any bin2-1 FG at stages FG0 and FG1 (Supplemental Figure S4A, S–D), suggesting that the abnormal vacuole observed in bin2-1 FG was not caused by early developmental processes and faulty cell fate specification. However, the ProFM1:GUS signal did not disappear in bin2-1 FG after stage FG1, indicating the transition between FM to FG might be disturbed (Supplemental Figure S4, E, S–H).

We next explored whether the vacuoles were initially formed at stage FG1, thus eventually leading to FG abortion, or whether FG development was first arrested at stage FG1, thereby resulting in vacuole formation. We introduced the vesicle and tonoplast-expressed marker ProUBQ10: GFP-VAMP711 into wild-type and bin2-1 mutant plants. Based on the growth of the inner and outer integuments, we divided stage FG1 into three substages (i.e. early, middle, and late stages of FG1). The outer integument is shorter than the inner integument at early stage FG1 (Figure 3, A and D), the outer integument is longer than the inner integument but does not enclose the nucellus at middle stage FG1 (Figure 3, B and E), and the outer integument encloses the nucellus but the inner integument does not at late stage FG1 (Figure 3, C and F). In wild-type FGs, GFP-VAMP711 signals were not detected at early and middle stages of FG1, but were detected at late stage FG1 (Figure 3, A–C), indicating that extremely small vacuoles formed, a result consistent with previous reports (Christensen et al., 1997). By contrast, in bin2-1 FGs, GFP-VAMP711 signals were first seen at early stage FG1, and they gradually fused during the middle and late stages of FG1, suggesting that small vacuoles had coalesced and formed larger vacuoles (Figure 3, D–F). These results demonstrated that the aberrant large vacuoles observed were formed in bin2-1 FG at early stage FG1.

The large vacuoles that form early block nuclear division at stage FG1

To study how the aberrant large vacuole affects FG development, we analyzed bin2-1 FGs at later developmental stages. At stage FG4, the wild-type FG gave rise to a four-nucleate embryo sac with a large central vacuole (Figure 1K). By contrast, many bin2-1 FGs were arrested at the one-nucleate stage and contained aberrant large vacuoles, indicating that the first nuclear division did not occur in these abnormal FGs (Figure 1L). At stage FG7, the wild-type FG developed into a typical four-celled embryo sac (Figure 1M), while approximately 52.6% ($n = 306$) of bin2-1 FGs degenerated (Figure 1, N and S), a proportion consistent with the total ratio of abnormal FGs at stage FG1 (about 43.6% containing large vacuoles and 9% degradation) (Figure 1Q). Similar
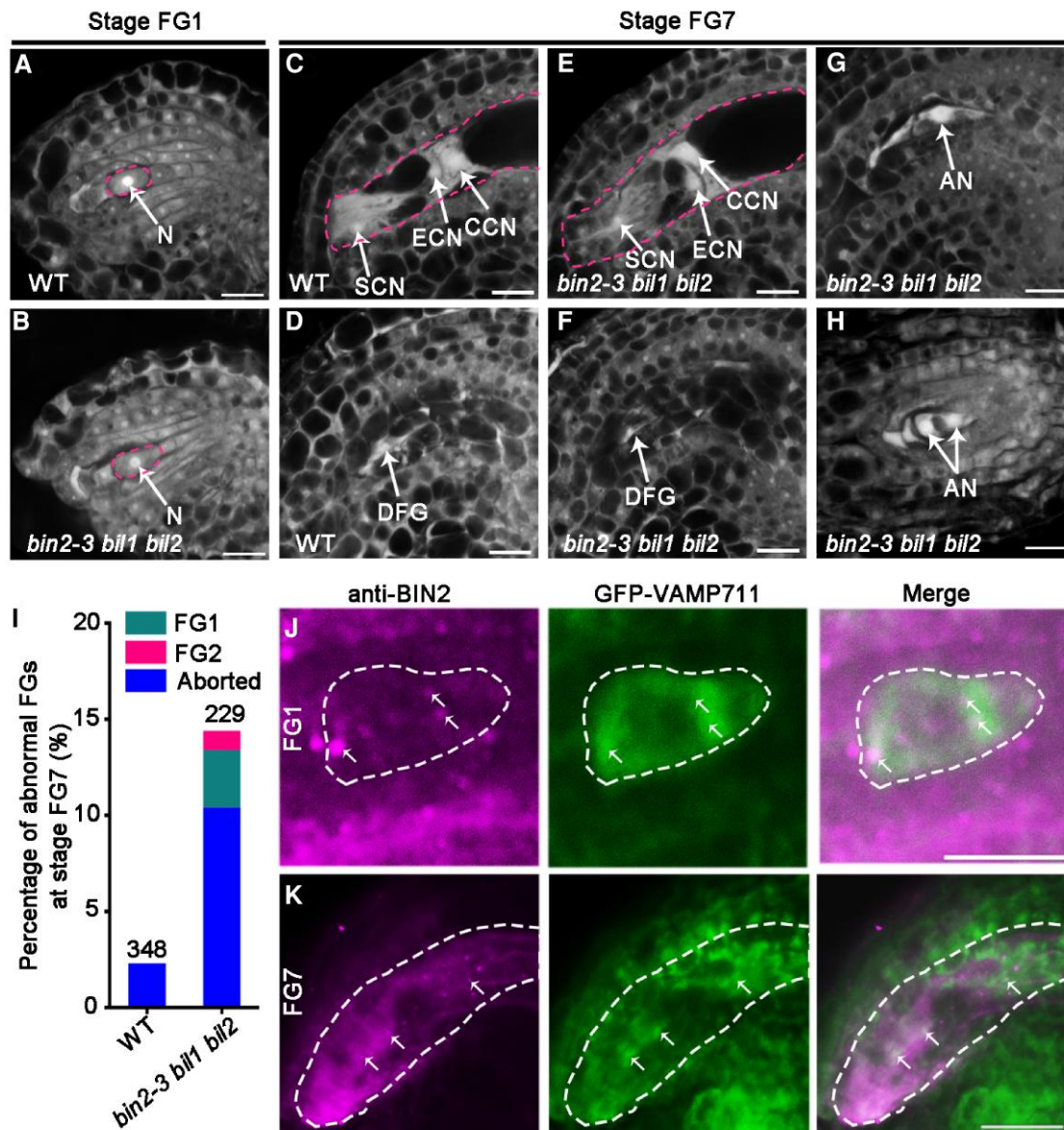
Figure 2 BIN2 is required for female gametophyte development. (A–I) Phenotypic analysis of FG development in the *bin2-3 bil1 bil2* triple mutant. (A) Wild-type FG at stage FG1 (Ws ecotype, the wild-type control for *bin2-3 bil1 bil2*). (B) *bin2-3 bil1 bil2* FG at stage FG1. (C–D) Mature (C) and aborted (D) FGs at stage FG7 in wild-type plants. (E–H) Images of *bin2-3 bil1 bil2* mutant at stage FG7 showing normal FGs (E), degenerated FGs (F), FGs arrested at stage FG1 (G), and FGs arrested at stage FG2 (H). (I) Percentages of abnormal FGs at stage FG7 in wild-type and *bin2-3 bil1 bil2* plants. Numbers represent how many FGs were detected for calculating the percentages. Dashed lines outline the FGs (A–C, E). N indicates the FG nuclei (A–B). CCN, ECN and SCN indicate the nuclei of central, egg, and synergid cells, respectively (C, E). DFG represents the degenerated FG exhibiting by their strong autofluorescence (D, F). AN represents the arrested nuclei at stage FG1 (G) or FG2 (H). (J–K) BIN2 localizes in a punctate pattern in FG at stage FG1 (J) and FG7 (K) revealed by immunolocalization assay, and partially co-localizes with the vesicle and tonoplast-expressed marker GFP-VAMP711. White dashed lines outline the FGs. White arrows indicate that BIN2 co-localizes with GFP-VAMP711. Bars = 10 μm.

results were also obtained for #31 and #32, in which almost all FGs degenerated (Figure 1, O, P, and S), displaying a more severe phenotype of ovule abortion (Supplemental Figure S1B). These results suggested that the presence of large vacuoles that formed early and blocked nuclear division are tightly connected, making it very possible that the large vacuoles at early stage FG1 affect nuclear division and finally lead to FG abortion in *bin2-1*.

This hypothesis was further supported by *ProFM1:GUS* staining, which in the wild-type was restricted to stage FG1 (Supplemental Figure S4, C and G), but remained later after stage FG1 in *bin2-1* (Supplemental Figure S4, D and H). This suggests that early formation of vacuoles disrupted FG development. In addition, bikinin and LiCl treatments significantly increased the percentage of mature *bin2-1* FGs at stage FG7 (Supplemental Figure S5), implying that inhibition of large
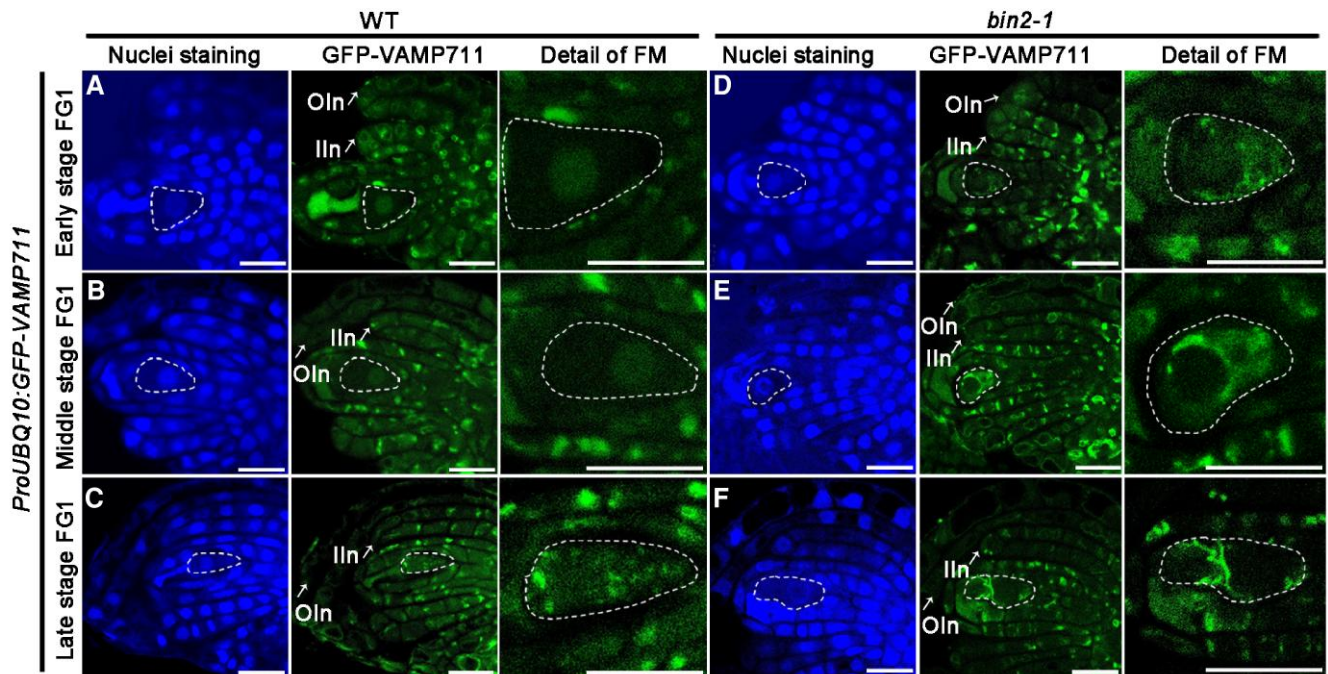
Figure 3 Early formation of large vacuoles impairs the female gametophyte development. (A–F) Expression of the vesicle and tonoplast-expressed marker *ProUBQ10:GFP-VAMP711* in wild-type (A–C) and *bin2-1* (D–F) FGs at the early (A, D), middle (B, E), and late (C, F) stages of FG1. Nuclei were stained with H33258. OIn and IIn indicate the outer and inner integuments, respectively. White dotted lines outline the FGs. Bars = 10 µm.

vacuole formation at stage FG1 could restore nuclear division (Figure 1R). Taken together, these results indicated that early formation of large vacuoles blocked the first nuclear division in FG and finally resulted in its abortion. Also, the chromosome behavior in the root apical meristem cells in *bin2-1* was not obviously affected (Supplemental Figure S6A, S–H), suggesting that BIN2 might regulate FG development without directly affecting the first mitosis at stage FG1.

BIN2 participates in female gametophyte development mainly by regulating vacuole formation

To investigate whether BIN2 is involved in other processes during FG development, we crossed a specific maker line of the egg cell *ProDD45:GFP* (Wu et al., 2012) with the *bin2-1* mutant. Expression of *ProDD45:GFP* was observed in normal *bin2-1* FGs at stage FG7, a result consistent with that of the wild-type, suggesting that the egg cell identity was not affected (Supplemental Figure S4, I and J). Because the *bin2-1* mutant could produce a few viable seeds (Supplemental Figure S1, B and C), we speculated that the cell fates of the central cell, synergid cells and antipodal cells were normal. These results suggested that BIN2 is involved in FG development mainly by regulating vacuole formation.

BIN2 interacts with VLG both in vitro and in vivo

To gain insight into how BIN2 regulates the vacuole formation and FG development, we performed RT-qPCR experiments to examine the expression levels of genes required

for the initiation of FG development, using *AtKIN-1* (Wang H et al., 2014), *Bub3.1* (Lermontova et al., 2008), *AGP18* (Acosta-Garcia and Vielle-Calzada, 2004), *ABORTED GAMETOPHYTE 1* (*AOG1*) (Cui et al., 2015), *MOS7* (Park et al., 2014), *AGL23* (Colombo et al., 2008), and cell cycle related genes including *CYCA1;1*, *CYCB2;3*, *CYCD2;1/3;1* (Menges et al., 2006; De Schutter et al., 2007; Hu et al., 2010; Eloy et al., 2011). None of them showed significantly changes in transcriptional levels in *bin2-1* (Supplemental Figure S7), suggesting that the block in FG development in *bin2-1* is unlikely caused by altered expression of these genes. Because *VLG* is known to promote vesicular fusion to form vacuoles during FG development (D'Ippólito et al., 2017), we speculated that it might be involved in the premature formation of large vacuoles in *bin2-1* FGs at stage FG1.

Because VLG localizes in MVBs/PVCs and promotes vesicular fusion to form large vacuoles in FGs (D'Ippólito et al., 2017), we speculated that BIN2 might participate in vacuole formation through interacting with VLG. Using a yeast two-hybrid system (Y2H), we verified their interaction (Figure 4A). Bimolecular fluorescence complementation (BiFC) assays illustrated that BIN2 interacted with VLG in the cytoplasm in a punctate pattern (Figure 4B). In an in vitro pull-down assay, recombinant maltose binding protein (MBP)-VLG bound to glutathione S-transferase (GST)-BIN2, but not to GST (Figure 4C). Similarly, co-immunoprecipitation (Co-IP) analysis also indicated that BIN2 interacted with VLG in *Arabidopsis* co-expressing *Pro35S:BIN2-MYC* and *Pro35S: VLG-GFP* (Figure 4D). In addition, BIN2 and VLG co-localized
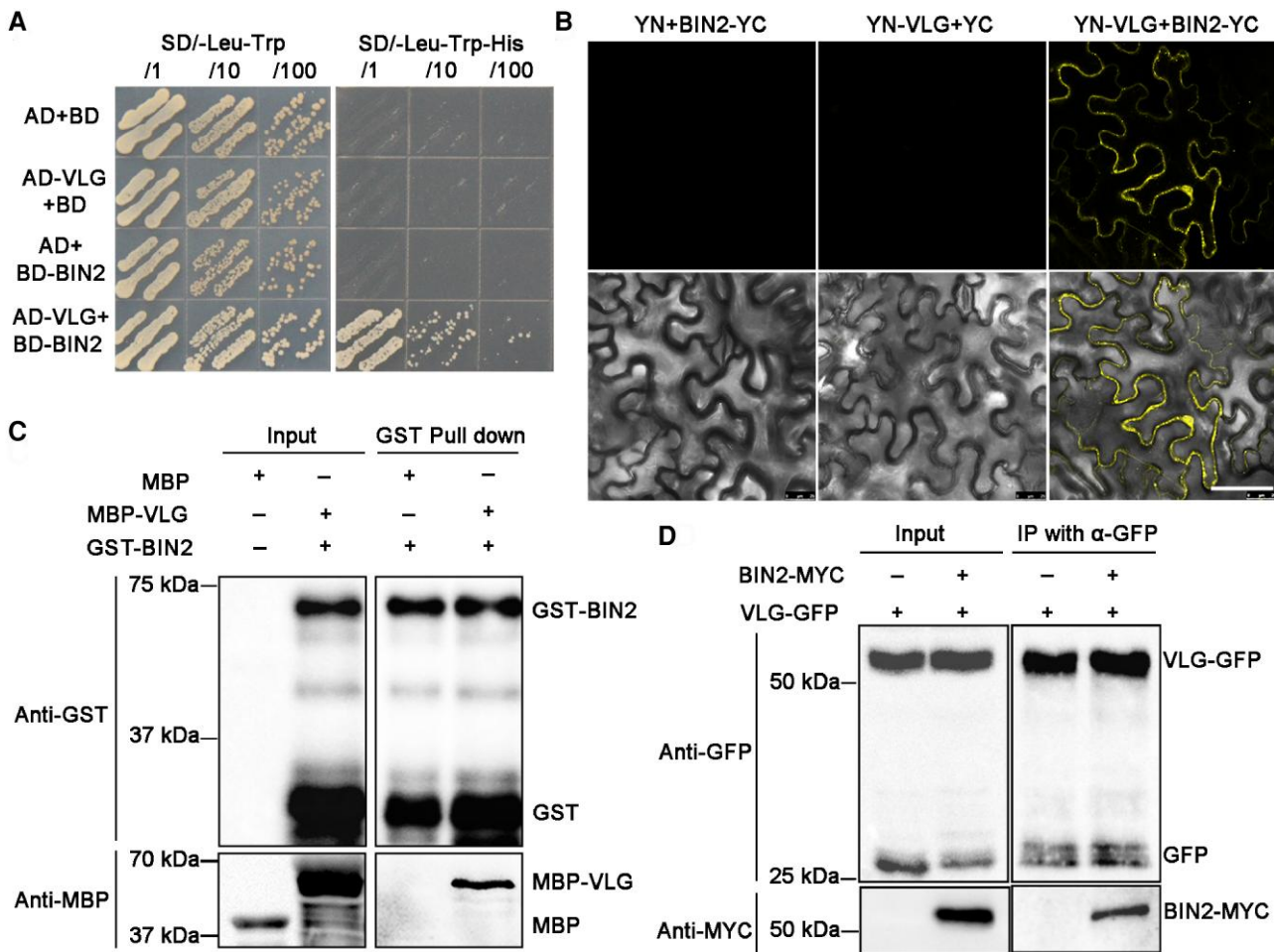
Figure 4 BIN2 interacts with VLG in vivo and in vitro. (A) Yeast two-hybrid assay indicates the interaction between BIN2 and VLG. Protein interactions are evaluated on YPD medium lacking Leu and Trp (left) or Leu, Trp, and His (right). (B) BiFC assay reveals the interaction between BIN2 and VLG. Bars = 50 µm. (C) *In vitro* pull-down assay indicates the direct interaction between GST-BIN2 and MBP-VLG. (D) *In vivo* co-immunoprecipitation assay reveals the interaction between BIN2-MYC and VLG-GFP.

in a punctate pattern in the cytoplasm of the *Nicotiana benthamiana* leaf epidermal cells (Supplemental Figure S8). Overall, we found that BIN2 and VLG are both expressed in the FG (Figure 2J–K, Supplemental Figures S2 and 3; D'Isppólito et al., 2017), that they interact with each other in vitro and in vivo, and that their mutant phenotypes phenocopy each other. Therefore, we predict that BIN2 and VLG function together in FG development.

BIN2 positively regulates VLG abundance and influences large vacuole formation

BIN2 participates in diverse cellular signal transduction pathways by affecting protein stability (Youn and Kim, 2015). To investigate whether BIN2 affects VLG stability, we generated transgenic plants expressing *Pro35S:VLG-GFP* in *bin2-1* and *bin2-3 bil1 bil2* mutants. Compared with the wild-type plants, the relative protein levels of VLG-GFP were significantly increased in *bin2-1* heterozygous and homozygous plants in a dosage-dependent

manner. In contrast, they were significantly reduced in *bin2-3 bil1 bil2* (Figure 5, A and B), indicating that BIN2 positively regulates VLG stability in vivo.

To examine whether high VLG abundance is responsible for the early formation of large vacuoles in *bin2-1* FG at stage FG1, we performed an RNA interference (RNAi) experiment using the *FM1* promoter to specifically knock down *VLG* expression (Kerschen et al., 2004; Huanca-Mamani et al., 2005). Two independent lines of *ProFM1:VLG-RNAi bin2-1* (#1 and #2) exhibited significantly decreased VLG expression (Supplemental Figure S9A), and the number of FGs at stage FG1 containing large vacuoles was significantly reduced (Figure 5C). This suggests that specifically knocking down *VLG* expression inhibited the early formation of large vacuoles at stage FG1. Meanwhile, specifically overexpressing a *ProFM1:VLG-GFP* construct in wild-type plants showing high VLG-GFP protein abundance resulted in the early formation of large vacuole at stage FG1 (Figure 5D; Supplemental Figure S9B). Importantly, the percentage of abnormal FGs at stage FG7 was significantly reduced in the
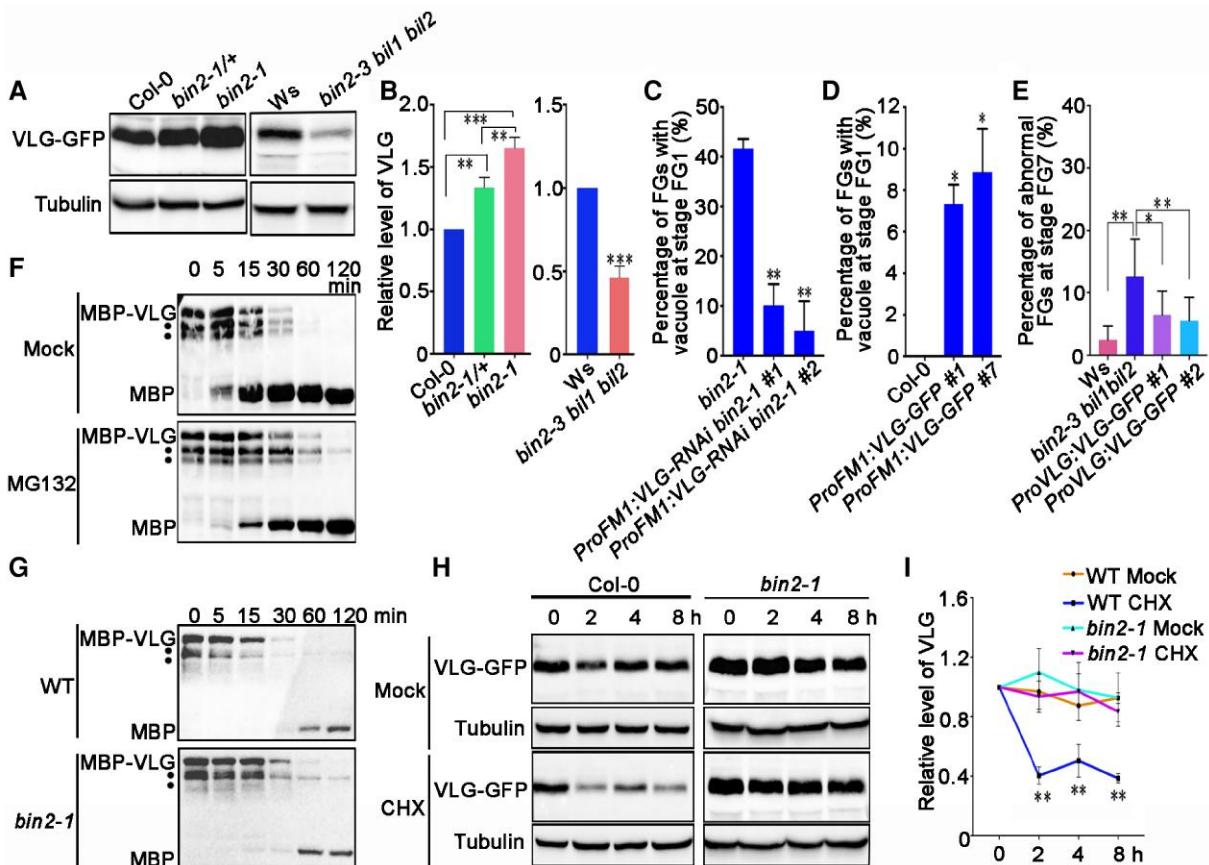
Figure 5 BIN2 regulates VLG stability. (A–B) VLG is more stable in *bin2-1* than wild-type and *bin2-3 bil1 bil2*. Representative immunoblot images (A), and statistical analysis of relative VLG-GFP protein levels (B). Total proteins were extracted from wild-type (Col-0 and Ws), *bin2-1* and *bin2-3 bil1 bil2* plants expressing *Pro35S:VLG-GFP*, respectively. VLG was detected using an anti-GFP antibody, and tubulin was used as an internal control. The integrated optical density (IOD) values of VLG and tubulin were quantified using Image Lab software (Bio-Rad). The relative protein levels of VLG were calculated by $IOD^{VLG}/IOD^{tubulin}$. Data represent means $\pm$ SD of three independent experiments. (C) Significantly reduced numbers of vacuole-containing FGs at stage FG1 in *ProFM1:VLG-RNAi bin2-1* plants. FGs from four independent pistils were analyzed for each line. (D) Significantly increased numbers of vacuole-containing FGs at stage FG1 in *ProFM1:VLG-GFP* transgenic plants. FGs from two independent pistils were examined for each line. (E) Percentages of abnormal FGs at stage FG7. #1 and #2 represent two independent lines expressing *ProVLG: VLG-GFP* in *bin2-3 bil1 bil2* mutant. FGs from 10 individual pistils were examined for each plant. (F) MG132 suppresses VLG degradation in a cell-free degradation assay. A mixture of MBP-VLG with wild-type protein extracts was incubated with mock (DMSO) or 100 μM MG132 for the indicated times, and was detected using an anti-MBP antibody. (G) VLG degradation was attenuated in *bin2-1* in a cell-free degradation assay. MBP-VLG was mixed with equal amounts of total protein extracts of wild-type and *bin2-1*, respectively. The mixture was incubated for the indicated times and detected with anti-MBP antibody. Dots indicate the degenerated MBP-VLG (F–G). (H–I) VLG was more stable in *bin2-1* than that in wild-type plants under 100 μM CHX treatment at indicated time. Representative immunoblot images (H) and statistical analysis (I). The relative abundance of VLG-GFP protein was analyzed as described for (A–B) and compared with $IOD^{VLG}/IOD^{tubulin}$ at 0 h. Data represent means $\pm$ SD of three independent experiments. Asterisks indicate the significant differences (*$P < 0.05$, **$P < 0.01$, ***$P < 0.001$, one-way ANOVA, Supplemental Data Set S2).

bin2-3 bil1 bil2 mutant expressing *ProVLG:VLG-GFP* (Figure 5E), indicating that VLG could partially restore *bin2-3 bil1 bil2* phenotype. These results suggest that VLG abundance influences vacuole formation.

BIN2 enhances VLG stability via phosphorylation

To investigate how VLG abundance is regulated, we conducted a cell-free degradation assay. Purified recombinant MBP-VLG proteins were incubated with total proteins extracted from wild-type plants, supplemented with or without MG132, a 26S proteasome inhibitor. The degradation rate of

VLG was higher in the mock controls than in MG132-treated samples (Figure 5F), suggesting that VLG is unstable and can be degraded by the 26S proteasome. Similarly, the degradation rate of VLG was higher in wild-type than in *bin2-1* (Figure 5G), revealing that BIN2 stabilizes VLG in vitro. We then investigated the stability of VLG in planta in the presence of the protein synthesis inhibitor cycloheximide (CHX). The relative protein levels of VLG-GFP were significantly decreased in wild-type, while not significantly affected in *bin2-1* mutant (Figure 5, H and I), indicating that VLG was more stable in *bin2-1* than in the wild-type. These results

suggest that BIN2 enhances VLG stability by protecting it from being degraded by the 26S proteasome.

Because BIN2 interacts with VLG, which contains three copies of the consensus S/T-X-X-X-S/T GSK3 phosphorylation motif (Wang et al., 2002; Ryu et al., 2007, 2010) (Figure 6, A and B), we investigated whether VLG could be phosphorylated by BIN2 in vitro. Phosphorylation assays using recombinant MBP-VLG and MBP-BIN2 proteins indicated that VLG was phosphorylated by BIN2 (Figure 6C). We then performed liquid chromatography-tandem mass spectrometry (LC-MS) analysis to identify the potential phosphorylation sites of VLG using recombinant MBP-VLG and MBP-BIN2 proteins. The results showed that BIN2 phosphorylates the T99, S103, S115, T119, S204, and S208 residues in the consensus GSK3 phosphorylation motif in VLG (Supplemental Figure S10). To confirm that these conserved residues in VLG are phosphorylated by BIN2, we simultaneously mutated T99, S103, S115, T119, S204, and S208 to Ala to create a phospho-defective version of VLG ($VLG^{S/T-A}$) or to Asp to create a phospho-mimetic version of VLG ($VLG^{S/T-D}$). Phosphorylation assays revealed that the phosphorylation of the $VLG^{S/T-A}$ mutated version by BIN2 was obviously reduced compared with wild-type VLG (Figure 6C). These results indicated that BIN2 phosphorylates VLG mainly through these residues.

To further verify that BIN2 stabilizes VLG via phosphorylation, we examined the effect of calf intestinal alkaline phosphatase (CIP) and commercial GSK3β on the stability of VLG protein in vitro. The results revealed that VLG abundance decreased in the presence of CIP but increased in the presence of GSK3β (Figure 6D), indicating that BIN2 promotes VLG stability via phosphorylation. In addition, when incubated with total proteins extracted from wild-type plants, the $VLG^{S/T-A}$ mutant protein was degraded more quickly than wild-type VLG, while the $VLG^{S/T-D}$ mutant protein was degraded more slowly (Figure 6E), suggesting that $VLG^{S/T-A}$ protein is relatively unstable and $VLG^{S/T-D}$ protein is rather stable. These results indicated that BIN2-mediated phosphorylation of VLG is required for its stability.

BIN2 might participate in large vacuole formation and female gametophyte development by phosphorylating VLG

We then investigated whether the VLG residues phosphorylated by BIN2 influence VLG function in FG development. We constructed transgenic plants expressing *ProFM1: $VLG^{S/T-A}$-GFP* and *ProFM1:$VLG^{S/T-D}$-GFP* in wild-type plants, respectively, and we observed FGs at stage FG1 of T1 transformants. In *ProFM1:$VLG^{S/T-D}$-GFP* transgenic plants, approximately 10% (#24) and 4.1% (#30) of FGs contained vacuoles, and 4.8% (#24) and 3.3% (#30) collapsed, exhibiting defects similar to those of *bin2-1* (Figure 7, A–E). In *ProFM1: $VLG^{S/T-A}$-GFP* transgenic plants, no obvious vacuoles were observed, while about 8.1% (#7) and 6.8% (#11) of FGs collapsed (Supplemental Figures S11, A–S and S1D), exhibiting

phenotypes similar to *bin2-3 bil1 bil2*, and *vlg/VLG* (D'Ippólito et al., 2017). It is likely that BIN2 is involved in large vacuole formation and FG development through phosphorylating VLG.

Taken together, the accumulation and degradation of VLG in wild-type FG is usually in balance (Figure 8A). Increased BIN2 activity in *bin2-1* enhances VLG protein stability through preventing its degradation by the 26S proteasome, thus promoting large vacuole early formation at stage FG1 (Figure 8B). By contrast, decreased activity of *BIN2* and its homologs in *bin2-3 bil1 bil2* promotes VLG degradation, resulting in impaired large vacuole formation at late developmental stage (Figure 8C). Both conditions result in defective FG (Figure 8, B and C). Collectively, our study revealed that the correct spatiotemporal formation of large vacuole regulated by BIN2-VLG is required for FG development.

Discussion

The formation of a large vacuole is critical for FG expansion and nuclear localization, and this large vacuole begins to form at late stage FG2 (Christensen et al., 1997). Several reports have indicated that interrupting formation of the large vacuole impairs FG development (Pischke et al., 2002; Panoli et al., 2015; D'Ippólito et al., 2017). Notably, VLG facilitates vesicular fusion to form large vacuoles, and the *vlg/VLG* mutant has pleiotropic defects in FG development, including arrest at stages FG1 or FG2, the lack of large central vacuole at stage FG5, or becoming collapsed at stage FG7 (D'Ippólito et al., 2017). We hypothesized that arrested nuclear division in *vlg/VLG* might be due to less (or later) formation of an obvious vacuole at stage FG2. Here, we reveal that the earlier formation of visible vacuoles at stage FG1 also disturbed FG development, indicating that the proper spatiotemporal pattern of vacuole formation is essential for embryo sac development.

BIN2 is a GSK3-like kinase and phosphorylates the conserved motif (S/T-X-X-X-S/T) of substrate proteins (Wang et al., 2002; Ryu et al., 2007, 2010), involving multiple signals during plant growth and development (Ye et al., 2019; Li et al., 2020; Song et al., 2021; Zhang et al., 2021). In this study, we discovered that BIN2 participates in vacuole formation in FG and influences FG development. Increased BIN2 activity triggered early vacuole formation at stage FG1 (Figure 1, C, F, I, Q), and this could be partially rescued by BIN2 inhibitors (Figure 1R). Loss of *BIN2* function in the *bin2-3 bil1 bil2* triple mutant led to fewer vacuoles at arrested two-nucleate FG (Figure 2H), and both *BIN2* mutants had arrested and collapsed FG. Most importantly, BIN2 phosphorylated specific residues in VLG, stabilizing VLG (Figure 6, C and E), and thus influenced vacuole formation and disturbed normal FG development. In addition, BIN2 and VLG could function together in FG, further supported their functions in vacuole formation. Therefore, these data uncovered a key regulator of VLG and further demonstrated that VLG modulates large vacuole formation in FG.
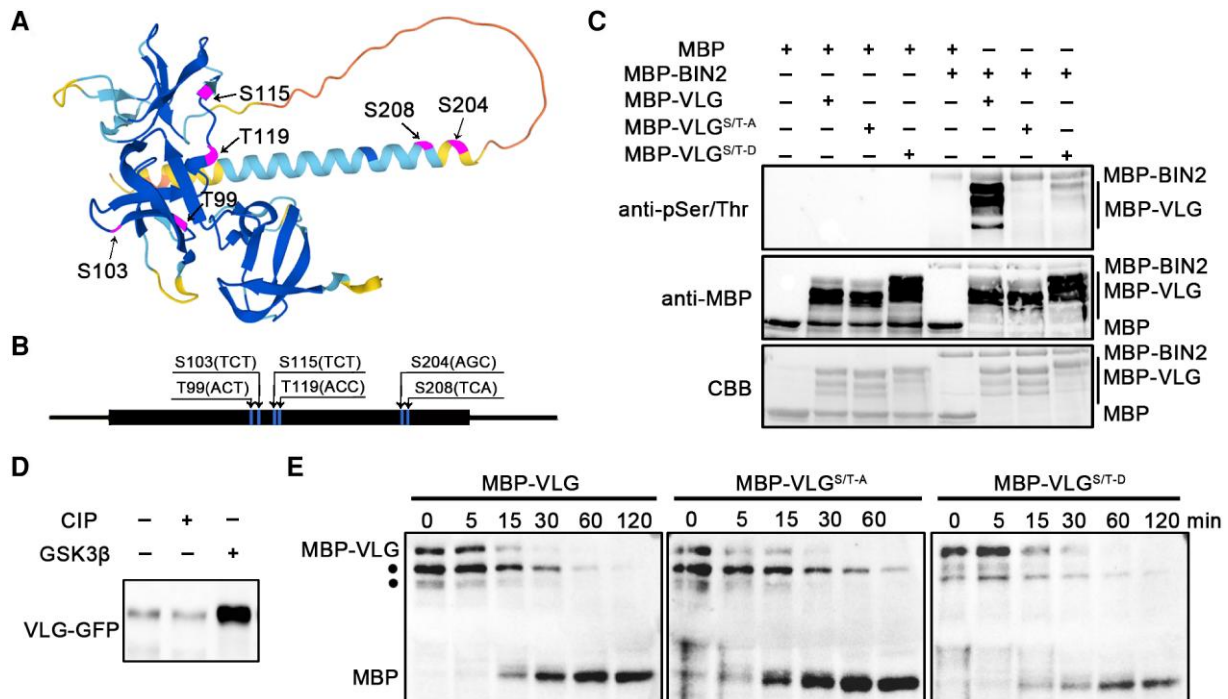
Figure 6 BIN2 increases the stability of VLG via phosphorylation. (A) Predicted structure of VLG protein by Alphafold 2 (https://www.alphafold.ebi.ac.UK). The arrows indicate the phosphorylated residues determined by mass spectrometry. (B) The translated open reading frame of VLG. The black box represents the protein-coding exon; thin lines denote untranslated regions. Arrows indicate the positions of the phosphorylated residues. C, BIN2 phosphorylates VLG. The phosphorylation of the phospho-defective protein MBP-VLG$^{S/T-A}$ by BIN2 was significantly decreased and attenuates its stability compared with wild-type VLG and the phospho-mimic protein MBP-VLG$^{S/T-D}$ in vitro. MBP, MBP-BIN2, MBP-VLG, and phosphorylation site-mutated MBP-VLG were immunoprecipitated and purified using anti-MBP-conjugated beads. Different combinations of purified proteins were mixed and incubated at 30°C. (D) VLG-GFP was less abundant following CIP treatment, but more abundant following GSK3β treatment in vitro. It was immunoprecipitated using anti-GFP-conjugated beads from *Pro35S:VLG-GFP* transgenic plants in wild-type, after which the beads were incubated with or without CIP or GSK3β. (E) The mutant protein MBP-VLG$^{S/T-A}$ was less stable while MBP-VLG$^{S/T-D}$ was more stable than wild-type MBP-VLG in vitro. MBP-VLG, MBP-VLG$^{S/T-A}$, and MBP-VLG$^{S/T-D}$ proteins were mixed with the wild-type protein extracts for the indicated times, respectively, and detected using an anti-MBP antibody. Dots indicate the degenerated MBP-VLG.

Our results illustrated how VLG stability can directly influence large vacuole formation in developing FGs. Specifically knocking down *VLG* expression in *bin2-1* FG at stage FG1 significantly reduced the percentage of vacuole-containing FGs, while overexpressing *VLG* promoted vacuole formation in wild-type FG at stage FG1 (Figure 5, C and D). Consistent with these results, specifically overexpressing a phospho-mimetic version of VLG accelerated vacuole formation at stage FG1 (Figure 7), and specifically overexpressing a phospho-defective version of VLG affected FG development (Supplemental Figure S11). This might be caused by competition between VLG$^{S/T-A}$ and wild-type VLG, resulting in a reduced amount of functional VLG. These results suggest that spatiotemporal formation of the large vacuole is tightly connected with VLG abundance. Therefore, the strict regulation of VLG abundance by BIN2 phosphorylation is required for spatiotemporal formation of large vacuole and FG development.

However, we noticed that VLG protein levels were considerably reduced in *bin2-3 bil1 bil2*, but not fully abolished (Figure 5, A and B), suggesting that BIN2 is likely not the only kinase that phosphorylates and stabilizes VLG. Previous study reported that two *Petunia hybrida* GSK3-like kinases PSK4 and PSK6 have been found to be highly expressed in FGs (Decroocq-Ferrant et al., 1995). This implies that other GSK3-like kinases also function in FG development as there are ten members in Arabidopsis (Jonak and Hirt, 2002). In addition, we cannot exclude the possibility that other regulators are involved in VLG-mediated vacuole formation and FG development because there are many other potentially phosphorylatable residues in VLG detected by mass spectrometry (MS) (Supplemental Figure S10).

The signals from the MMC and FM markers illustrated that the identity of MMC and FM is normal in *bin2-1*, while the first nuclear division is blocked in part of *bin2-1* FGs, indicating that BIN2 regulates the first nuclear division (Supplemental Figure S4, A, S–H). The expression of the egg cell marker suggested that the remaining part of *bin2-1* FGs develop to mature FGs (small number of seeds) and that the identity of egg cells in these FGs is normal (Supplemental Figure S4, I and 4). Based on the above results,
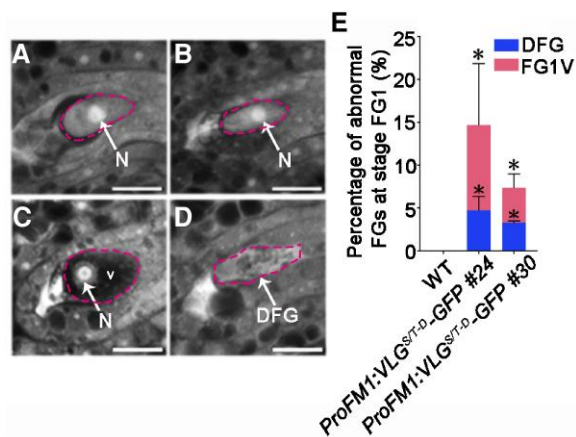
Figure 7 The expression of site-mutated VLG protein leads to abnormal female gametophyte development. (A) Wild-type FG at stage FG1. B–D, Normal (B), abnormal with vacuoles (C), and collapsed (D) FGs at stage FG1 in *ProFM1:VLG^{S/T-D}-GFP* transformants. (E) Percentages of the distinct phenotypes at stage FG1. FGs from four independent pistils were analyzed for each line. Dashed lines outline the FGs. N represents the nuclei. DFG indicates the degenerated FGs. FG1V, FG containing vacuoles at stage FG1. Bars = 10 μm. Error bars represent means ± SD. Significant differences were determined by one-way ANOVA (*$P < 0.05$, Supplemental Data Set S2).

we propose that BIN2 does not affect FG cell identity. The signal of GFP-VAMP711 in wild-type and *bin2-1* suggested that vacuoles were formed early, before FG development in *bin2-1* (Figure 3A–F), and that early vacuole formation is the reason but not the result of impaired FG development in *bin2-1*.

Another interesting phenomenon is that site-mutated VLG still interacts with BIN2 (Supplemental Figure S12), suggesting that mutation of these phosphorylation residues did not affect their interaction, but did influence VLG stability. VLG localizes to the MVBs/PVCs, which act as the intermediate compartments between the *trans*-Golgi network (TGN) and the vacuole. MVBs/PVCs enable proteins to be recycled before MVBs/PVCs fusion with the vacuole (Cui et al., 2016, 2020). It suggested that increased or decreased VLG abundance may disturb the balance between protein recycling and MVBs/PVCs fusion with the vacuole. Therefore, we propose that increased activity of BIN2-VLG module promotes vacuole early formation at stage FG1, while decreased activity of BIN2-VLG module leads to delay or less vacuole formation at stage FG2. Both of these two conditions impair FG development, and it is likely that an increased level of the BIN2-VLG module has more severe influence.

Importantly, using inhibitor treatments, genetic experiments, and *ProFM1:GUS* expression, we verified that the large vacuoles forming early at stage FG1 block the first nuclear division in the embryo sac or the initiation of FG development (Figures 1, 3, and 5). Still, how FG development is triggered after the FM forms remains largely unclear. Our data revealed that the mitotic chromosome behavior in root apical meristem cells of *bin2-1* did not have obvious defects

(Supplemental Figure S6), and the transcription levels of genes relevant to cell cycle regulation and mitosis were not changed in *bin2-1* (Supplemental Figure S7), indicating blocked nuclear division of FG possibly because of the micro-environmental cue. Since the large vacuole formation is known as a fact regulating embryo sac expansion and nuclear location, it is likely that the early formed large vacuole disturbs the normal location of the nucleus and normal micro-environment at stage FG1; therefore, the regular signaling between micro-environment and the nucleus is interrupted, and nuclear division program cannot be triggered. A recent publication reported that positional signal determines the cell fate of the cells in embryo sac (Sun et al., 2021), indicating that the exact position of the nuclei in embryo sac is critical for cell behavior and fates. Our work provides evidence that the proper position of the nucleus in one-nucleate embryo sac is critical for the initiation of its division and is useful for further investigations on the possible positional cues for the initiation of FG generation. Taken together, our study demonstrated that BIN2-regulated VLG stability is a new regulatory mechanism for FG vacuole formation, and spatiotemporal formation of large vacuole mediated by BIN2-VLG module is required for normal FG development.

Materials and methods

Plant materials and growth conditions

Plants were grown, transformed, and screened as previously described (Clough and Bent, 1998; Zu et al., 2019). Wild-type ecotypes of *Arabidopsis thaliana* used include Col-0, Ws-2, and Ler. Most materials used in this work are in the Col-0 ecotype, including *bin2-1* (Li et al., 2001), *ProDD45:GFP* (Wu et al., 2012), *ProFM1:GUS* (Huanca-Mamani et al., 2005; Yu et al., 2020), *ProSTK:BIN2*-GFP* (Zu et al., 2019), and *Pro35S:BIN2-MYC* (Ye et al., 2019). The *bin2-3 bil1 bil2* triple mutant (Yan et al., 2009) is in the Ws-2 ecotype, and *ProKNU:KNU-VENUS* is in the Ler ecotype (Payne et al., 2004; Zhao et al., 2018). All Arabidopsis plants were grown in the nutrient-rich soil in a greenhouse at 22°C and a long-day cycle (16 h light/8 h dark) with the fluorescent white light at 90 μmol m^{-2} s^{-1} (FSL LED T8-16-65/A22B/24 bulb).

DNA manipulation

The *ProUBQ10:GFP-VAMP711* construct was generated using Gateway technology (Invitrogen). Entry vectors produced from the pENTR/D/TOPO vector (Invitrogen) were used for attL-left and attR-right (LR) reactions involving the destination vector containing *ProUBQ10:GFP-GW* to generate *ProUBQ10:GFP-VAMP711*. All other constructs in this study were produced using the One Step Cloning Kit (Vazyme).

To generate the *Pro35S:VLG-GFP* construct, a 747-bp fragment of the *VLG* coding sequence (CDS) was amplified and introduced into the pCAMBIA1302 vector (Zhang et al., 2022) between *Bgl*II and *Spe*I sites. *BIN2* promoter and
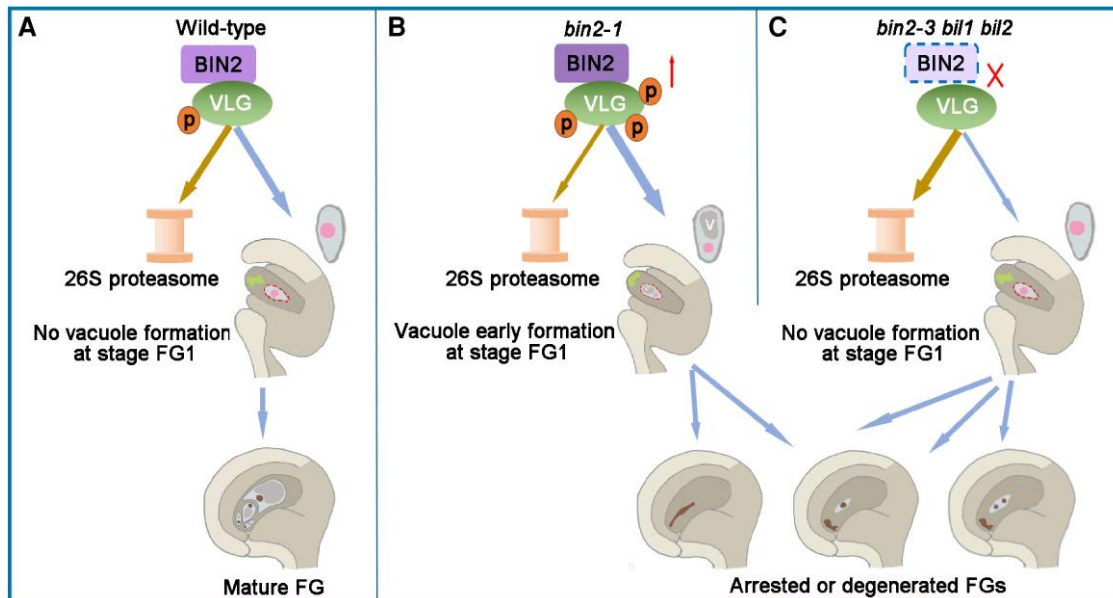
Figure 8 Proposed model for how the BIN2-VLG module influences female gametophyte development by regulating vacuole formation at an early developmental stage. (A) In wild-type plants, the accumulation and degradation of VLG is usually in balance. There are no visible large vacuoles in FG at stage FG1. (B) In *bin2-1*, increased BIN2 activity enhances VLG stability through preventing its degradation by the 26S proteasome via phosphorylating VLG. This promotes large vacuole formation in FG at stage FG1, resulting in defective FG development. (C) In the *bin2-3 bil1 bil2* triple mutant, decreased BIN2 activity reduces VLG stability, leading to smaller vacuoles in FGs at stage FG2, causing defective FG development. Taken together, our study revealed that BIN2 stabilizes VLG by interacting and phosphorylating VLG, and the correct spatiotemporal formation of vacuoles regulated by BIN2-VLG module is required for normal FG development. The arrow and fork represent the enhanced interaction and the loss of interactions between BIN2 and VLG, respectively. P indicates protein phosphorylation.

genomic fragments were amplified according to a previous report (Li and Nam, 2002), and were cloned into the *pHB* vector (Xu et al., 2019) between *Eco*RI and *Bam*HI sites to generate *ProBIN2:BIN2-GFP* construct. To produce the destination vectors *ProUBQ10:GW-mCherry*, *ProVLG:GW-GFP*, and *ProFM1:GW-GFP*, the CaMV 35S promoter in *pHB* was replaced by the *UBQ10*, *VLG*, and *FM1* promoters, respectively. Then, the fragments of *BIN2* and *VLG* were amplified to generate *ProUBQ10:BIN2-mCherry*, *ProFM1:VLG-GFP*, *ProVLG:VLG-GFP*, respectively. To construct the *ProFM1:VLG-RNAi* plasmid, both the *FM1* promoter and a 481-bp *VLG*-sense fragment were amplified and mixed with the *pFGC5941* plasmid (Huanca-Mamani et al., 2005) digested with *Eco*RI and *Nco*I. The mixture underwent reactions using the multi-step Cloning Kit (Vazyme), after which the *VLG*-antisense cDNA fragment was amplified and inserted into the *Bam*HI cloning site. The underlined sites of VLG CDS (295 ACTTACAATTGTTCT 309, 343 TCTGTGCCTGAGACC 357, 610 AGCTCCGCGAATTCA 624) that encode the conserved phosphorylation amino acid residues (S/T) were replaced by (295 GATTACAATTGTGAT 309, 343 GATGTGCCT GAGGAC 357, 610 GACTCCGCGAATGAT 624) that encode a phosphor-mimetic amino acid residue (D), respectively, for *ProFM1:VLG$^{S/T-D}$-GFP* construct, and replaced by (295 GCTTACAATTGTGCT 309, 343 GCTGTGCCTGAGGCC 357, 610 GCCTCCGCGAATGCA 624) that encode a phosphor-defective amino acid residue (A), respectively, for *ProFM1:VLG$^{S/T-A}$-GFP* construct. The relative fragments

were amplified individually and were cloned into the *pHB* vector as described above.

For the BiFC assays, the destination vectors were *ProXY104: GW-cYFP* and *ProXY106:nYFP-GW* and were used to generate the expression vectors *ProXY104:BIN2-cYFP* and *ProXY106: nYFP-VLG*. For the Y2H assays, the destination vectors were *pGBKT7* and *pGADT7* (Xu et al., 2019), which were used to generate the expression vectors *pGBKT7-BIN2* and *pGADT7-VLG*. For the pull-down and in vitro phosphorylation assays, the *VLG* and *BIN2* CDS were cloned and inserted into *pMAL-C2X* vector (Chen et al., 2021) to obtain the plasmid expressing the recombinant protein MBP-VLG and MBP-BIN2. The *pGEX40-BIN2* plasmid expressing the recombinant protein GST-BIN2 was described previously (Ye et al., 2019).

All PCR amplifications were performed using PrimeSTAR GXL DNA polymerase (Takara). The PCR procedure was set as recommended by the manufacturer (95°C 5 min; 98°C 15 s, 60°C 20 s, 68°C 1–4 min according to the fragment length, 34 cycles; 68°C 5 min; 4°C, 5 min). The vectors were sequenced and analyzed using DNAMAN. All primers are listed in Supplemental Data Set S1.

Total RNA extraction and RT-qPCR
Total RNA was extracted from Arabidopsis inflorescences using the TRIzol reagent (Invitrogen), after which 2 μg RNA was used to synthesize first-strand cDNA using the FastKing RT Kit with gDNase (Tiangen). The RT-qPCR experiments were performed using the SYBR Green Realtime PCR

Master Mix (TOYOBO) and the Thermo Fisher QuanStudio 3 RealTime PCR Apparatus. *ACTIN7* (At5G09810) was served as an internal control (Zu et al., 2019; Jiang et al., 2020). All experiments comprised two independent experimental runs, each comprising three technical replicates. Primer sequences are listed in Supplemental Data Set S1.

Confocal laser scanning microscopy

Ovules were examined by confocal laser scanning microscopy according to a previously described method (Christensen et al., 1997; Shi et al., 2005). Dissected pistils were fixed under vacuum for 30 min in 4% glutaraldehyde prepared in 12.5 mM cacodylate (pH 6.9). They were then incubated in fixative solution at room temperature overnight. Samples were dehydrated in the following ethanol series: 10%, 20%, 40%, 60%, 80%, and 90% (10 min per step). After an overnight incubation in 90% ethanol, the tissues were washed twice for at least 10 min in 100% ethanol until they were completely decolorized. The tissues were cleared in 2:1 (v/v) benzyl benzoate:benzyl alcohol for at least 1 h. Ovules were separated from pistils and mounted in immersion oil, after which they were examined using the Leica TCS SP8 microscope at excitation and emission wavelengths of 488 nm and 505–550 nm, respectively.

Treatment assays

For 10 μM bikinin and 10 mM LiCl treatments, *bin2-1* floral buds larger than floral stage 11 were removed (Smyth et al., 1990), then the treatment solutions were added to the soil. After 7 days, the ovule phenotypes were examined by confocal laser scanning microscopy. For CHX treatment, 3-week-old leaves were collected and incubated in half strength Murashige and Skoog (1/2× MS) medium (Murashige and Skoog, 1962) containing with or without 100 μM CHX for specific time periods.

Whole-mount immunolocalization assay

Pistils at floral stage 12b to 13 were dissected to expose the ovules (Christensen et al., 1997). The immunolocalization assay was performed according to a previous reported method (Escobar-Guzmán et al., 2015). BIN2 (Agrisera, Rabbit, AS163203) and GFP (Agrisera, Rabbit, AS152987) primary antibodies were used at a dilution of 1:100. An Alexa Fluor 488-conjugated AffiniPure Goat Anti-Rabbit IgG (H + L) and an Alexa Fluor 594-conjugated AffiniPure Goat Anti-Rabbit IgG (H + L) secondary antibodies (Jackson ImmunoResearch) were used at a dilution of 1:300. Fluorescence was observed using a confocal laser scanning microscopy (Leica TCS SP8).

Histological analysis

For H33258 staining assay (Laube and Kiderlen, 1998; Maiti et al., 2009), dissected pistils were incubated in a fixative solution (4% paraformaldehyde in PBS solution containing 137 mM NaCl, 2.7 mM KCl, 10 mM Na_2HPO_4, 2 mM KH_2PO_4, pH 7.4) under vacuum conditions at room temperature for 1 h. The pistils were rinsed three times in PBS, and mounted in 200 μL ClearSee solution (Kurihara et al., 2015) until they were completely bleached, following by washing three times. The samples were immersed in H33258 staining buffer (5 μg mL^{-1} in PBS) at 22°C for 30 min in darkness and then washed three times in PBS. The isolated ovules were examined using a Leica TCS SP8 laser scanning microscope with a 405-nm diode laser. The band pass (410–460 nm) filter was set for H33258 scanning. For GUS staining assays, dissected pistils from plants of *ProFM1:GUS* transgenic lines were collected and prepared as previously described (Zu et al., 2019). The ovules were examined using the Axio Imager M2 differential interference contrast microscopy (Zeiss, Göttingen, Germany).

Protein interaction assays

The Y2H analysis was performed as previously described (Wang et al., 2011). Yeast strain AH109 cells (Clontech) were co-transformed with the two plasmids and then cultured on SC medium containing glucose, but lacking leucine and tryptophan. The co-transformed yeast cells were screened on SC medium containing glucose, but lacking leucine, tryptophan, and histidine (SC/−Leu/−Trp/−His). For BiFC analysis, associated vectors were transformed into *Agrobacterium tumefaciens* strain GV3101 cells, which were then used to infiltrate *Nicotiana benthamiana* tobacco leaf epidermal cells. The tobacco leaves were incubated in darkness for 48–72 h, and YFP fluorescence was examined by confocal laser scanning microscopy (Leica TCS SP8).

To purify the recombinant proteins used for the in vitro pull-down experiment, *pMAL-C2X-VLG* and *pGEX40-BIN2* were transformed into BL21 competent cells (DE3), which were cultured in LB medium containing 100 μg mL^{-1} ampicillin at 37°C until the OD_{600} reached 0.5–0.8. Protein expression was induced by adding isopropyl-β-D-1-thiogalactopyranoside to a final concentration of 0.5 mM. Cells were incubated overnight at 16°C in a horizontal shaker with 180 rpm. The bacterial culture was centrifuged at 18,514 g for 10 min at 4°C. The pelleted cells were resuspended in 1×PBS and lysed by sonification on ice. The solution was centrifuged at 18,514 g for 10 min at 4°C to eliminate cellular debris. The MBP-VLG or GST-BIN2 recombinant proteins in the supernatant were purified using dextrin beads 6FF (Smart-Lifesciences, cat. no. SA026025) or glutathione beads 4FF (Smart-Lifesciences, cat. no. SA010025), respectively. For the in vitro pull-down assay, MBP-VLG (1 μg) and GST-BIN2 (1 μg) were incubated with 10 μL pre-washed glutathione beads 4FF at 4°C for 3 h. After six washes with 1× PBS buffer, the beads were mixed with loading buffer and then boiled at 100°C for 10 min. A 30-μL aliquot of each boiled sample was used for the sodium dodecyl sulfate-polyacrylamide gel electrophoresis (SDS-PAGE) and immunoblot analysis using the anti-MBP antibody (Abways; cat. no. AB0029; 1:3000 dilution) and the anti-GST antibody (Abways; cat. no. AB0055; 1:3000 dilution).

For Co-IP assays, 0.1 g Arabidopsis leaves co-expressing *Pro35S:VLG-GFP* and *Pro35S:BIN2-MYC* were collected. Leaf

cell pellets were resuspended in lysis NB1 buffer [50 mM Tris-HCl, pH 8.0, 500 mM sucrose, 1 mM MgCl$_2$, 10 mM EDTA, 5 mM DTT, 2 mM PMSF, and 1× protease inhibitor cocktail (Roche)], and lysed on ice for 30 min. The solution was centrifuged at 18,514 g for 10 min at 4°C, after which the supernatant was collected and filtered through two layers of Miracloth (Calbiochem) to remove cellular debris. The proteins were incubated with 10 μL pre-washed anti-GFP-conjugated beads (Chromoek) for 3 h at 4°C. After six washes with NB1 buffer, the beads were mixed with loading buffer and boiled at 100°C for 10 min. A 30-μL aliquot of each boiled sample was analyzed by immunoblotting using the anti-MYC antibody (Abways; cat. no. AB0001; 1:3000 dilution) and the anti-GFP antibody (Abways; cat. no. AB0005; 1:3000 dilution).

Cell-free degradation assay

For cell-free degradation analysis, 0.1 g of 7-day-old seedlings were put in liquid nitrogen immediately and ground into a powder using Multi sample freeze grinder (Wonbio-Mini). Seedling cell pellets were resuspended in lysis buffer (25 mM Tris-HCl, pH 7.5, 10 mM NaCl, 10 mM MgCl$_2$, 5 mM DTT, 0.4 mM PMSF, and 10 mM ATP) and lysed on ice for 30 min. Next, 1 μg MBP-VLG recombinant protein was incubated with individual extracts in darkness at 22°C for specific time periods. The samples were mixed with loading buffer and boiled at 100°C for 10 min followed by SDS-PAGE. The anti-MBP antibody (Abways; cat. no. AB0029; 1:3000 dilution) was used to analyze protein degradation.

CIP and GSK treatment assays

For the CIP treatment, VLG-GFP was immunoprecipitated as described above. The GFP-conjugated beads were washed by NB1 and CIP buffers (three times each) and then incubated with 2 μL Quick CIP (New England Biolabs) in 500 μL CIP buffer (50 mM Tris-HCl, pH 7.5, 5 mM MgCl$_2$, 1 mM DTT, 1 mM PMSF, and 0.1% NP-40) for 60 min at 37°C. The beads were washed six times with CIP buffer. For the GSK3β treatment, VLG-GFP was immunoprecipitated as described above. The GFP-conjugated beads were washed six times with NB1 buffer and then incubated with 2 μL GSK3β in 300 μL GSK3β assay buffer for 60 min at 37°C as recommended by the manufacturer (SignalChem). The beads were washed six times with NB1 buffer and mixed with loading buffer, and then boiled at 100°C for 10 min. A 20-μL aliquot of each boiled sample was analyzed by immunoblotting using an anti-GFP antibody (Abways; cat. no. AB0005; 1:3000 dilution).

In vitro kinase treatment assay

MBP-VLG and MBP-BIN2 were immunoprecipitated and purified using MBP-conjugated beads as described above. 5 μg MBP or MBP-BIN2 proteins were incubated with 20 μg purified MBP or MBP-VLG at 30°C for 1 h. The corresponding purified proteins were incubated with phosphorylation buffer (25 mM Tris-HCl at pH 7.4, 12 mM MgCl$_2$, 1 mM DTT and

1 mM ATP) (Ye et al., 2019). They were then mixed with loading buffer, and boiled at 100°C for 10 min. A 15-μL aliquot of each boiled sample was analyzed by immunoblotting using the anti-MBP antibody (Abways; cat. no. AB0029; 1:3000 dilution), anti-Phosphor-(Ser/Thr) antibody (Abcam; cat. no. AB17464; 1:4,000 dilution).

Immunoblot assay

For total protein extraction, equal amounts of 7-day-old seedlings were grounded into fine powder as described above, and then resuspended in 2× SDS buffer. The samples were lysed on ice for 30 min, then centrifuged at 18,514 g for 10 min at 4°C. The supernatants were transferred into new tubes, and heated in boiling water for 10 min. 10 μL of total protein extracts were separated via 10% SDS-PAGE and then transferred to Protran nitrocellulose membranes (Whatman). The immunoblots were performed using an anti-BIN2 antibody (Agrisera; cat. no. AS163203; 1:5,000 dilution) in Supplemental Figure S2B, and an anti-GFP antibody (Abways; cat. no. AB0005; 1:5,000 dilution) and an anti-Tubulin antibody (Abmart, cat. no. M20045; 1:5,000 dilution) in Figure 5, A and H at 4°C overnight. The secondary antibodies used were Goat anti-mouse IgG (H + L) HRP (ShareBio; SB-AB0102; 1:5,000) or Goat anti-Rabbit IgG (H + L) HRP (ShareBio; SB-AB0101; 1:5,000). All antibodies were diluted in 5% skim milk powder (in PBS containing 1% Tween-20). The images were taken using the BIO-RAD ChemiDoc Imaging System. The integrated optical density (IOD) values of VLG and tubulin protein band signals in Figure 5, A and H were quantified using Image Lab software (Bio-Rad) (Ye et al., 2019).

Root mitosis analysis

Plants were grown on 1/2×MS medium for 7–10 days. Roots were fixed in Carnoy's fixative solution (100% ethanol:glacial acetic acid = 3:1) (Wang Y et al., 2014) for more than 1 h at room temperature. The fixed roots were washed three times with ddH$_2$O and then incubated in a digestion cocktail for 20 min at 37°C. The digested roots were placed on glass slides, and the root tips were separated using fine needles. The rest of the roots were discarded. After adding one drop of ddH$_2$O, the root tips were lysed by pinching several times with a pair of forceps. The slides were placed on a heat block at 45°C for 30 s, after which 20 μL of 60% acetic acid was added. The meiotic chromosomes were dispersed by adding 20-μL pre-chilled (−20°C) Carnoy's fixative solution to the center of the samples. The slides were dried on a heat block for 5–10 min. After adding 7–10 μl of DAPI, a cover slip was placed on top of the samples, which were then examined using the AxioScope A2 microscope (Wang Y et al., 2014).

Accession numbers

The accession numbers of genes discussed in this article are *ACTIN7* (At5G09810), *AGP18* (AT4G37450), *AGL23* (AT1G65360), *AOG1* (AT5G57790), *ATKIN-1* (At3G63480), *BIN2* (AT4G18710), *BIL1* (AT2G30980), *BIL2* (AT1G06390), *BUB3.1* (AT3G19590), *CYCA1;1* (AT1G44110), *CYCB2;3*

(AT1G20610), *CYCD2;1* (AT2G22490), *CYCD3;1* (AT4G34160). *DD45* (AT2G21740), *DYAD* (AT5G51330), *FM1* (AT4G12250), *KNU* (AT5G14010), *MOS7* (At5g05680), *PRL* (AT4G02060), *SNAIL1* (AT5G61770), *SWA1* (AT2G47990), *SWA2* (AT1G 72440), and *VLG* (AT2G17740).

Supplemental data

The following materials are available in the online version of this article.

Supplemental Figure S1. Vegetative growth and seed set in wild-type and BIN2-enhanced plants.

Supplemental Figure S2. *BIN2* is expressed in the female gametophyte.

Supplemental Figure S3. Subcellular localization of BIN2 in the female gametophyte.

Supplemental Figure S4. The expression of cell identity markers in wild-type plants and the *bin2-1* mutant.

Supplemental Figure S5. Female gametophyte defects were partially rescued by bikinin and LiCl treatments.

Supplemental Figure S6. Analysis of mitotic chromosome behavior in root apical meristem cells.

Supplemental Figure S7. Transcription levels of known regulators of female gametophyte development in *bin2-1*.

Supplemental Figure S8. Co-localization of BIN2 and VLG in *Nicotiana benthamiana* leaf epidermal cells.

Supplemental Figure S9. Expression analysis of *VLG* in transgenic plants.

Supplemental Figure S10. Identification of phosphorylation sites of VLG by mass spectrometry (MS).

Supplemental Figure S11. Phenotypic analysis of female gametophytes in *ProFM1:VLG$^{S/T-A}$-GFP* transgenic plants.

Supplemental Figure S12. Specific mutations of phosphorylatable residues in VLG do not affect their interactions with BIN2.

Supplemental Data Set S1. Primers used in this study.

Supplemental Data Set S2. Summary of statistical analyses.

References

Acosta-García G, Vielle-Calzada JP (2004) A classical arabinogalactan protein is essential for the initiation of female gametogenesis in Arabidopsis. Plant Cell **16**(10): 2614–2628

Chen Y, Shen J, Zhang L, Qi H, Yang L, Wang H, Wang J, Wang Y, Du H, Tao Z, et al. (2021) Nuclear translocation of OsMFT1 that is impeded by OsFTIP1 promotes drought tolerance in rice. Mol Plant **14**(8): 1297–1311

Christensen CA, King EJ, Jordan JR, Drews GN (1997) Megagametogenesis in *Arabidopsis* wild type and the *Gf* mutant. Sex Plant Reprod **10**(1): 49–64

Clough SJ, Bent AF (1998) Floral dip: a simplified method for Agrobacterium-mediated transformation of Arabidopsis thaliana. Plant J **16**(6): 735–743

Colombo M, Masiero S, Vanzulli S, Lardelli P, Kater MM, Colombo L (2008) AGL23, A type I MADS-box gene that controls female gametophyte and embryo development in Arabidopsis. Plant J **54**(6): 1037–1048

Cui HH, Liao HZ, Tang Y, Du XY, Chen LQ, Ye D, Zhang XQ (2015) *ABORTED GAMETOPHYTE 1* is required for gametogenesis in *Arabidopsis*. J Integr Plant Biol **57**(12): 1003–1016

Cui Y, Shen J, Gao C, Zhuang X, Wang J, Jiang L (2016) Biogenesis of plant prevacuolar multivesicular bodies. Mol Plant **9**(6): 774–786

Cui Y, Zhao Q, Hu S, Jiang L (2020) Vacuole biogenesis in plants: how many vacuoles, how many models? Trends Plant Sci **25**(6): 538–548

Decroocq-Ferrant V, Van Went J, Bianchi MW, de Vries SC, Kreis M (1995) Petunia hybrida homologues of shaggy/zeste-white 3 expressed in female and male reproductive organs. Plant J **7**(6): 897–911

De Rybel B, Audenaert D, Vert G, Rozhon W, Mayerhofer J, Peelman F, Coutuer S, Denayer T, Jansen L, Nguyen L, et al. (2009) Chemical inhibition of a subset of Arabidopsis thaliana GSK3-like kinases activates brassinosteroid signaling. Chem Biol **16**(6): 594–604

De Schutter K, Joubès J, Cools T, Verkest A, Corellou F, Babiychuk E, Van Der Schueren E, Beeckman T, Kushnir S, Inzé D, De Veylder L (2007) *Arabidopsis* WEE1 kinase controls cell cycle arrest in response to activation of the DNA integrity checkpoint. Plant Cell **19**(1): 211–225

D'Ippólito S, Arias LA, Casalongué CA, Pagnussat GC, Fiol DF (2017) The DC1-domain protein VACUOLELESS GAMETOPHYTES is essential for development of female and male gametophytes in Arabidopsis. Plant J **90**(2): 261–275

Ebine K, Fujimoto M, Okatani Y, Nishiyama T, Goh T, Ito E, Dainobu T, Nishitani A, Uemura T, Sato MH, et al. (2011) A membrane trafficking pathway regulated by the plant-specific RAB GTPase ARA6. Nat Cell Biol **13**(7): 853–859

Eloy NB, de Freitas Lima M, Van Damme D, Vanhaeren H, Gonzalez N, De Milde L, Hemerly AS, Beemster GTS, Inzé D, Ferreira PCG (2011) The APC/C subunit 10 plays an essential role in cell proliferation during leaf development. Plant J **68**(2): 351–363

Escobar-Guzmán R, Rodríguez-Leal D, Vielle-Calzada JP, Ronceret A (2015) Whole-mount immunolocalization to study female meiosis in Arabidopsis. Nat Protoc **10**(10): 1535–1542

Feng QN, Song SJ, Yu SX, Wang JG, Li S, Zhang Y (2017) Adaptor protein-3-dependent vacuolar trafficking involves a subpopulation

of COPII and HOPS tethering proteins. Plant Physiol **174**(3): 1609–1620

Gomez MD, Barro-Trastoy D, Fuster-Almunia C, Tornero P, Alonso JM, Perez-Amador MA (2020) Gibberellin-mediated RGA-LIKE1 degradation regulates embryo sac development in Arabidopsis. J Exp Bot **71**(22): 7059–7072

Hu ZB, Qin ZX, Wang M, Xu CY, Feng GP, Liu J, Meng Z, Hu YX (2010) The Arabidopsis SMO2, a homologue of yeast TRM112, modulates progression of cell division during organ growth. Plant J **61**(4): 600–610

Huanca-Mamani W, Garcia-Aguilar M, León-Martínez G, Grossniklaus U, Vielle-Calzada JP (2005) CHR11, A chromatin-remodeling factor essential for nuclear proliferation during female gametogenesis in Arabidopsis thaliana. Proc Natl Acad Sci U S A **102**(47): 17231–6

Jiang HL, Hong J, Jiang YT, Yu SX, Zhang YJ, Shi JX, Lin WH (2020) Genome-Wide association analysis identifies candidate genes regulating seed number per silique in *Arabidopsis thaliana*. Plants (Basel) **9**(5): 585

Jonak C, Hirt H (2002) Glycogen synthase kinase 3/SHAGGY-like kinases in plants: an emerging family with novel functions. Trends Plant Sci **7**(10): 457–461

Kerschen A, Napoli CA, Jorgensen RA, Müller AE (2004) Effectiveness of RNA interference in transgenic plants. FEBS Lett **566**(1–3): 223–228

Kim TW, Guan S, Sun Y, Deng Z, Tang W, Shang JX, Sun Y, Burlingame AL, Wang ZY (2009) Brassinosteroid signal transduction from cell-surface receptor kinases to nuclear transcription factors. Nat Cell Biol **11**(10): 1254–1260

Klein PS, Melton DA (1996) A molecular mechanism for the effect of lithium on development. Proc Natl Acad Sci U S A **93**(16): 8455–8459

Kooiker M, Airoldi CA, Losa A, Manzotti PS, Finzi L, Kater MM, Colombo L (2005) BASIC PENTACYSTEINE1, a GA binding protein that induces conformational changes in the regulatory region of the homeotic Arabidopsis gene SEEDSTICK. Plant Cell **17**(3): 722–729

Kurihara D, Mizuta Y, Sato Y, Higashiyama T (2015) Clearsee: a rapid optical clearing reagent for whole-plant fluorescence imaging. Development **142**(23): 4168–4179

Latrasse D, Benhamed M, Henry Y, Domenichini S, Kim W, Zhou DX, Delarue M (2008) The MYST histone acetyltransferases are essential for gametophyte development in Arabidopsis. BMC Plant Biol **8**(1): 121

Laube U, Kiderlen AF (1998) Detection of parasites with DNA-binding bisbenzimide H33258 in pneumocystis carinii- and leishmania-containing materials. Parasitol Res **84**(7): 559–564

Lermontova I, Fuchs J, Schubert I (2008) The Arabidopsis checkpoint protein Bub3.1 is essential for gametophyte development. Front Biosci **13**(13): 5202–5211

Li J, Nam KH, Vafeados D, Chory J (2001) BIN2, A new brassinosteroid-insensitive locus in Arabidopsis. Plant Physiol **127**(1): 14–22

Li J, Terzaghi W, Gong Y, Li C, Ling JJ, Fan Y, Qin N, Gong X, Zhu D, Deng XW (2020) Modulation of BIN2 kinase activity by HY5 controls hypocotyl elongation in the light. Nat Commun **11**(1): 1592

Li JM, Nam KH (2002) Regulation of brassinosteroid signaling by a GSK3/SHAGGY-like kinase. Science **295**(5558): 1299–1301

Liu F, Li JP, Li LS, Liu Q, Li SW, Song ML, Li S, Zhang Y (2021) The canonical α-SNAP is essential for gametophytic development in Arabidopsis. PLoS Genet **17**(4): e1009505

Liu J, Zhang Y, Qin G, Tsuge T, Sakaguchi N, Luo G, Sun K, Shi D, Aki S, Zheng N, et al. (2008) Targeted degradation of the cyclin-dependent kinase inhibitor ICK4/KRP6 by RING-type E3 ligases is essential for mitotic cell cycle progression during Arabidopsis gametogenesis. Plant Cell **20**(6): 1538–1554

Maiti S, Maiti P, Sinha SS, Mitra RK, Pal SK (2009) Molecular recognition of plant DNA: does it differ from conventional animal DNA? Int J Biol Macromol **44**(2): 133–137

Matias-Hernandez L, Battaglia R, Galbiati F, Rubes M, Eichenberger C, Grossniklaus U, Kater MM, Colombo L (2010) VERDANDI Is a direct target of the MADS domain ovule identity complex and affects embryo sac differentiation in Arabidopsis. Plant Cell **22**(6): 1702–1715

Menges M, Samland AK, Planchais S, Murray JAH (2006) The D-type cyclin CYCD3;1 is limiting for the G1-to-S-phase transition in *Arabidopsis*. Plant Cell **18**(4): 893–906

Modrusan Z, Reiser L, Feldmann KA, Fischer RL, Haughn GW (1994) Homeotic transformation of ovules into carpel-like structures in Arabidopsis. Plant Cell **6**(3): 333–349

Murashige T, Skoog F (1962) A revised medium for rapid growth and bio assays with tobacco tissue cultures. Physiol Plant **15**(3): 473–497

Panoli A, Martin MV, Alandete-Saez M, Simon M, Neff C, Swarup R, Bellido A, Yuan L, Pagnussat GC, Sundaresan V (2015) Auxin import and local auxin biosynthesis are required for mitotic divisions, cell expansion and cell specification during female gametophyte development in Arabidopsis thaliana. PLoS One **10**(5): e0126164

Park GT, Frost JM, Park JS, Kim TH, Lee JS, Oh SA, Twell D, Brooks JS, Fischer RL, Choi Y (2014) Nucleoporin MOS7/Nup88 is required for mitosis in gametogenesis and seed development in Arabidopsis. Proc Natl Acad Sci U S A **111**(51): 18393–8

Payne T, Johnson SD, Koltunow AM (2004) KNUCKLES (KNU) encodes a C2H2 zinc-finger protein that regulates development of basal pattern elements of the Arabidopsis gynoecium. Development **131-**(15): 3737–3749

Pinyopich A, Ditta GS, Savidge B, Liljegren SJ, Baumann E, Wisman E, Yanofsky MF (2003) Assessing the redundancy of MADS-box genes during carpel and ovule development. Nature **424**(6944): 85–88

Pischke MS, Jones LG, Otsuga D, Fernandez DE, Drews GN, Sussman MR (2002) An Arabidopsis histidine kinase is essential for megagametogenesis. Proc Natl Acad Sci U S A **99**(24): 15800–5

Rozhon W, Wang W, Berthiller F, Mayerhofer J, Chen T, Petutschnig E, Sieberer T, Poppenberger B, Jonak C (2014) Bikinin-like inhibitors targeting GSK3/shaggy-like kinases: characterisation of novel compounds and elucidation of their catabolism in planta. BMC Plant Biol **14**(1): 172

Ryu H, Cho H, Kim K, Hwang I (2010) Phosphorylation dependent nucleocytoplasmic shuttling of BES1 is a key regulatory event in brassinosteroid signaling. Mol Cells **29**(3): 283–290

Ryu H, Kim K, Cho H, Park J, Choe S, Hwang I (2007) Nucleocytoplasmic shuttling of BZR1 mediated by phosphorylation is essential in Arabidopsis brassinosteroid signaling. Plant Cell **19**(9): 2749–2762

Schneitz K, Hülskamp M, Pruitt RE (1995) Wild-type ovule development in Arabidopsis thaliana: a light microscope study of cleared whole-mount tissue. Plant J **7**(5): 731–749

Shi DQ, Liu J, Xiang YH, Ye D, Sundaresan V, Yang WC (2005) SLOW WALKER1, essential for gametogenesis in Arabidopsis, encodes a WD40 protein involved in 18S ribosomal RNA biogenesis. Plant Cell **17**(8): 2340–2354

Smyth DR, Bowman JL, Meyerowitz EM (1990) Early flower development in Arabidopsis. Plant Cell **2**(8): 755–767

Song Y, Zhai YH, Li LX, Yang ZE, Ge XY, Yang ZR, Zhang CJ, Li FG, Ren MZ (2021) BIN2 negatively regulates plant defence against *Verticillium dahliae in Arabidopsis* and cotton. Plant Biotechnol J **19**(10): 2097–2112

Stambolic V, Ruel L, Woodgett JR (1996) Lithium inhibits glycogen synthase kinase-3 activity and mimics wingless signalling in intact cells. Curr Biol **6**(12): 1664–1668

Sun Y, Wang X, Pan L, Xie F, Dai B, Sun M, Peng X (2021) Plant egg cell fate determination depends on its exact position in female gametophyte. Proc Natl Acad Sci U S A **118**(8): e2017488118

Tucker MR, Okada T, Hu Y, Scholefield A, Taylor JM, Koltunow AM (2012) Somatic small RNA pathways promote the mitotic events of megagametogenesis during female reproductive development in Arabidopsis. Development **139**(8): 1399–1404

Vert G, Chory J (2006) Downstream nuclear events in brassinosteroid signalling. Nature **441**(7089): 96–100

Wang H, Liu R, Wang J, Wang P, Shen Y, Liu G (2014) The Arabidopsis kinesin gene AtKin-1 plays a role in the nuclear division process during megagametogenesis. Plant Cell Rep **33**(5): 819–828

Wang J, Guo X, Xiao Q, Zhu J, Cheung AY, Yuan L, Vierling E, Xu S (2021) Auxin efflux controls orderly nucellar degeneration and expansion of the female gametophyte in Arabidopsis. New Phytol **230**(6): 2261–2274

Wang Y, Cheng Z, Lu P, Timofejeva L, Ma H (2014) Molecular cell biology of male meiotic chromosomes and isolation of male meiocytes in Arabidopsis thaliana. Methods Mol Biol **1110**: 217–230

Wang Z, Meng P, Zhang X, Ren D, Yang S (2011) BON1 Interacts with the protein kinases BIR1 and BAK1 in modulation of temperature-dependent plant growth and cell death in Arabidopsis. Plant J **67**(6): 1081–1093

Wang ZY, Nakano T, Gendron J, He J, Chen M, Vafeados D, Yang Y, Fujioka S, Yoshida S, Asami T, et al. (2002) Nuclear-localized BZR1 mediates brassinosteroid-induced growth and feedback suppression of brassinosteroid biosynthesis. Dev Cell **2**(4): 505–513

Webb MC, Gunning BES (1990) Embryo sac development in Arabidopsis thaliana. Sex Plant Reprod **3**(4): 244–256

West M, Harada JJ (1993) Embryogenesis in higher plants: an overview. Plant Cell **5**(10): 1361–1369

Wu JJ, Peng XB, Li WW, He R, Xin HP, Sun MX (2012) Mitochondrial GCD1 dysfunction reveals reciprocal cell-to-cell signaling during the maturation of Arabidopsis female gametes. Dev Cell **23**(5): 1043–1058

Xiong F, Duan CY, Liu HH, Wu JH, Zhang ZH, Li S, Zhang Y (2020) Arabidopsis *KETCH1* is critical for the nuclear accumulation of ribosomal proteins and gametogenesis. Plant Cell **32**(4): 1270–1284

Xu P, Lian H, Xu F, Zhang T, Wang S, Wang W, Du S, Huang J, Yang HQ (2019) Phytochrome B and AGB1 coordinately regulate photomorphogenesis by antagonistically modulating PIF3 stability in Arabidopsis. Mol Plant **12**(2): 229–247

Yan Z, Zhao J, Peng P, Chihara RK, Li J (2009) BIN2 Functions redundantly with other Arabidopsis GSK3-like kinases to regulate brassinosteroid signaling. Plant Physiol **150**(2): 710–721

Ye K, Li H, Ding Y, Shi Y, Song C, Gong Z, Yang S (2019) BRASSINOSTEROID-INSENSITIVE2 Negatively regulates the stability of transcription factor ICE1 in response to cold stress in Arabidopsis. Plant Cell **31**(11): 2682–2696

Youn JH, Kim TW (2015) Functional insights of plant GSK3-like kinases: multi-taskers in diverse cellular signal transduction pathways. Mol Plant **8**(4): 552–565

Yu SX, Zhou LW, Hu LQ, Jiang YT, Zhang YJ, Feng SL, Jiao Y, Xu L, Lin WH (2020) Asynchrony of ovule primordia initiation in *Arabidopsis*. Development **147**(24): dev196618

Zhang DW, Tan WR, Yang F, Han Q, Deng XG, Guo HQ, Liu BH, Yin YH, Lin HH (2021) A BIN2-GLK1 signaling module integrates brassinosteroid and light signaling to repress chloroplast development in the dark. Dev Cell **56**(3): 310–324.e7

Zhang YJ, Zhang Y, Zhang LL, He JX, Xue HW, Wang JW, Lin WH (2022) The transcription factor OsGATA6 regulates rice heading date and grain number per panicle. J Exp Bot **73**(18): 6133–6149

Zhao L, Cai H, Su Z, Wang L, Huang X, Zhang M, Chen P, Dai X, Zhao H, Palanivelu R, et al. (2018) *KLU* Suppresses megasporocyte cell fate through SWR1-mediated activation of *WRKY28* expression in *Arabidopsis*. Proc Natl Acad Sci U S A **115**(3): E526–EE35

Zu SH, Jiang YT, Hu LQ, Zhang YJ, Chang JH, Xue HW, Lin WH (2019) Effective modulating brassinosteroids signal to study their specific regulation of reproductive development and enhance yield. Front Plant Sci **10**: 980